

# Galaxy Evolution in Cosmological Simulations With Outflows I: Stellar Masses and Star Formation Rates

Romeel Davé<sup>1</sup>, Benjamin D. Oppenheimer<sup>2</sup>, Kristian Finlator<sup>3</sup>

<sup>1</sup> *Astronomy Department, University of Arizona, Tucson, AZ 85721, USA*

<sup>2</sup> *Veni Fellow; Leiden Observatory, Leiden University, PO Box 9513, 2300 RA Leiden, Netherlands*

<sup>3</sup> *Hubble Fellow; Physics Department, University of California, Santa Barbara, CA 93106, USA*

15 January 2013

## ABSTRACT

We examine the growth of the stellar content of galaxies from  $z = 3 \rightarrow 0$  in cosmological hydrodynamic simulations incorporating parameterised galactic outflows. Without outflows, galaxies overproduce stellar masses ( $M_*$ ) and star formation rates (SFRs) compared to observations. Winds introduce a three-tier form for the galaxy stellar mass and star formation rate functions, where the middle tier depends on differential (i.e. mass-dependent) recycling of ejected wind material back into galaxies. A tight  $M_*$ –SFR relation is a generic outcome of all these simulations, and its evolution is well-described as being powered by cold accretion, although current observations at  $z \gtrsim 2$  suggest that star formation in small early galaxies must be highly suppressed. Roughly one-third of  $z = 0$  galaxies at masses below  $M^*$  are satellites, and star formation in satellites is not much burstier than in centrals. All models fail to suppress star formation and stellar mass growth in massive galaxies at  $z \lesssim 2$ , indicating the need for an external quenching mechanism such as black hole feedback. All models also fail to produce dwarfs as young and rapidly star-forming as observed. An outflow model following scalings expected for momentum-driven winds broadly matches observed galaxy evolution around  $M^*$  from  $z = 0 - 3$ , which is a significant success since these galaxies dominate cosmic star formation, but the failures at higher and lower masses highlight the challenges still faced by this class of models. We argue that central star-forming galaxies are well-described as living in a slowly-evolving equilibrium between inflows from gravity and recycled winds, star formation, and strong and ubiquitous outflows that regulate how much inflow forms into stars. Star-forming galaxy evolution is thus primarily governed by the continual cycling of baryons between galaxies and intergalactic gas.

**Key words:** galaxies: formation, assembly, low redshift; intergalactic medium; cosmology: theory; methods: numerical

## 1 INTRODUCTION

Galaxies are the primary tracers by which astronomers map and measure the Universe, so understanding how galaxies form and evolve is a longstanding central goal of astronomy. The physics of galaxy formation involves a diverse set of processes spanning an enormous dynamic range, from black holes and stellar physics on sub-parsec scales to cosmology and large-scale structure on gigaparsec scales. As a consequence, despite rapidly advancing observations of galaxies across cosmic time, a comprehensive theory for the formation and evolution of galaxies that can explain all their observed properties remains elusive.

As galaxies are essentially collections of stars, understanding the growth of the stellar component of galaxies

is of fundamental importance. Recent observations have probed the star formation rates and stellar masses of galaxies out to redshift  $z \sim 7$ . Key trends have emerged. For instance, fairly massive galaxies are in place at early epochs, and galaxies exhibit “downsizing” in the sense that more massive galaxies form their stars earlier and have lower birthrates today. While some claim that these trends are in conflict with expectations from hierarchical structure formation, they are actually not. Since the most massive galaxies form within the largest mass density peaks, they collapse first and start forming stars earlier than lower-mass systems (Davé et al. 2006; Neistein, van den Bosch, & Dekel 2006). The collapse is driven by gravitational instability and strong radiative cooling that (left unchecked) grow galax-

ies very rapidly at early epochs, so that models without strong feedback yield galaxies that are *too large* at high redshifts (e.g. Davé, Finlator, & Oppenheimer 2006). It is important to note that no confirmed high- $z$  galaxy yet observed is too large to be produced in a hierarchical model, and in fact strong feedback appears to be necessary to suppress galaxy formation from the earliest epochs. The evolution of galaxy stellar masses and star formation rates therefore provide valuable insights into the processes, particularly related to feedback, that drive galaxy formation from the highest redshift until today.

The canonical scenario for galaxy formation posits that galaxies assemble first as rotationally-supported disks cooling out of virial-temperature gas within a dark matter halo (e.g. Rees & Ostriker 1977; White & Rees 1978; White & Frenk 1991), and then such objects merge to form larger and earlier-type systems (e.g. Mihos & Hernquist 1996). Naively, one expects then that star-forming disks would be surrounded by hot gaseous halos (Benson et al. 2000), and that early low-mass objects would tend to be disk-like while more massive objects would be ellipticals. Recent observations, however, do not clearly support this paradigm. For instance, star-forming disks and hot (X-ray emitting) gaseous halos are rarely if ever found together (e.g. Rasmussen et al. 2009, though see Crain et al. 2010 and references therein). Observed dynamics of  $z \sim 1-2$  galaxies indicate that larger objects tend to be disk-like, while smaller ones are dispersion-dominated (Förster Schreiber et al. 2009). Furthermore, galaxies appear to be consuming their gas rapidly enough that fuel must be constantly replenished (Tacconi et al. 2010; Papovich et al. 2010), but merger-induced starbursts do not appear to be driving global star formation (Brinchmann et al. 2004; Noeske et al. 2007; Jogee et al. 2009). Hence there is some doubt that the canonical halo/merger-centric view provides the appropriate framework for galaxy formation, despite the wide-ranging successes that models based on this have enjoyed (e.g. Benson 2010).

Improvements in cosmological hydrodynamic simulations over the past decade have made them a competitive approach towards understanding the physics of galaxy formation in a hierarchical structure formation context. The complex three-dimensional geometry of large-scale structure is self-consistently evolved together with the baryonic components that make up observable galaxies and the co-evolving intergalactic medium (IGM). These simulations have long suggested that accretion onto galaxies is powered by cold, filamentary streams that connect to the cosmic web on larger scales (Kereš et al. 2005; Dekel et al. 2009), and that most accreted gas fueling star formation never heats to the virial temperature (Katz & Gunn 1991; Dekel & Birnboim 2006). Gas replenishment from the IGM is a natural outcome of this model, and generally occurs smoothly rather than being driven by major mergers (e.g. Murali et al. 2002; Kereš et al. 2005; van de Voort et al. 2010). These simulations provide many insights into how galaxies form and grow, some of which are in common with the traditional scenario, while some differ.

Recently, simulations incorporating strong and ubiquitous outflows have had success matching a wide range of data on galaxies (e.g. Davé, Finlator, & Oppenheimer 2006; Finlator & Davé 2008; Oppenheimer et al. 2010) and

the IGM (e.g. Oppenheimer & Davé 2006, 2008, 2009; Oppenheimer, Davé, & Finlator 2009). The outflow models in these simulations were originally tuned to enrich the IGM in accord with observations of  $z \sim 2-4$  C IV absorbers (Oppenheimer & Davé 2006). The favoured scalings turn out to be those expected for momentum-conserved winds (Murray, Quataert, & Thompson 2005; Zhang & Thompson 2010), namely that the wind speed scales with circular (or escape) velocity, while the amount of mass ejected per unit star formation (i.e. the mass loading factor) scales inversely with it. This provides sufficiently early IGM enrichment by expelling the majority of metals formed in small high-redshift galaxies, while having moderate wind speeds that does not to overheat the IGM (Oppenheimer & Davé 2006). In subsequent work we showed that an outflow model with similar scalings consistently does as well or better than any other outflow model that we have tried at matching a wide range of IGM properties. We note that the actual implementation of this wind model in our simulations has evolved owing to advances in modeling techniques and changes in cosmology (Oppenheimer & Davé 2008; Oppenheimer et al. 2010). Successes include very early ( $z \gtrsim 5$ ) enrichment (Oppenheimer, Davé, & Finlator 2009), O VI absorbers at low- $z$  (with the introduction of a physically-motivated IGM turbulence model Oppenheimer & Davé 2009), the metallicities in intragroup and intracluster gas (Davé, Oppenheimer, & Sivanandam 2008), and the overall cosmic metal distribution (including the so-called “missing metals problem”; Davé & Oppenheimer 2007).

Examining galaxy properties, we again found that an outflow model following similar scalings was the most successful amongst the ones we tried. Successes included matching the mass-metallicity relation at  $z = 2$  (Finlator & Davé 2008), the shape of the present-day stellar mass function (Oppenheimer et al. 2010) below  $M^*$ , damped Ly $\alpha$  absorber kinematics (Hong et al. 2010), and observations of very high- $z$  ( $z \gtrsim 4$ ) galaxies (Finlator et al. 2006; Davé, Finlator, & Oppenheimer 2006; Bouwens et al. 2007; Finlator et al. 2010). This is not to say that this particular outflow model matches all the data; in fact, it does not, it simply does better than others attempted, including the oft-used Springel & Hernquist (2003b) model. Moreover, the implementation remains highly heuristic, and may be impacted by numerical effects (e.g. see discussion in Oppenheimer et al. 2010). Nevertheless, the consistent (comparative) success of an outflow model with momentum-driven wind scalings suggests that it captures some essential ingredients required for a successful model of galactic outflows, and motivates a more detailed investigation of the implications of such outflows.

Two key predictions from models incorporating outflows with such scalings are that (i) the total amount of material ejected from galaxies significantly exceeds that going into stars (Oppenheimer & Davé 2008, hereafter OD08); and (ii) the ejected material often re-accretes onto galaxies (Oppenheimer et al. 2010). The strong and ubiquitous ejection and re-accretion of material suggest that galaxies are best viewed as evolving within an ecosystem of surrounding intergalactic gas with which they continually exchange mass, energy, and metals.

While the above results are encouraging, these simu-

lations have yet to be comprehensively tested against observations of galaxy evolution from the present epoch back into the early universe. Such a comparison would provide the most stringent test to date of how well these simulations can reproduce the observed Universe, and would better highlight the current successes and failures of galaxy evolution simulations. This series of papers aims to understand how basic galaxy statistics and scaling relations between their stellar, gas, and metal content constrain the physics of galaxy formation. In Paper I (this paper) we focus on the statistics of and scaling relations between stellar mass and star formation rate. In Paper II (Davé, Finlator, & Oppenheimer, in prep.) we will additionally investigate the gas and metal content of galaxies. The primary goal of these works is to understand and characterise the key physical processes that drive the observable properties of galaxies across cosmic time.

In these papers, we will demonstrate that for a particular choice of outflow model, namely outflows following scalings as expected for momentum-driven winds, the simulations can reproduce key observations of scaling relations between stars, gas, and metals for large star-forming galaxies that dominate cosmic star formation. This is a first for cosmological hydrodynamic simulations. However, all simulations we examine here fail to match selected galaxy properties at high and low masses, indicating that additional or different physics is required even for our most successful model. Using insights gained from the simulations, we show that relations between basic galaxy constituents can be broadly understood through a simple scenario in which inflows are balanced by outflows and star formation. This contrasts with the canonical halo/merger-centric model of galaxy formation; in our scenario, the dark matter halo's virial radius and galaxy mergers play a sub-dominant role in the evolution of star-forming systems. We argue that galactic outflows are the key moderator of the stellar content, star formation rate, and gas and metal evolution in galaxies at all epochs. In turn, observations of these properties provide valuable constraints on the cosmic ecosystem within which galaxies form and grow.

This paper is organised as follows. In §2 we describe our hydrodynamic simulations including our galactic outflow model. In §3 we investigate the galaxy stellar mass and star formation rate functions, and explain the three-tier behavior generically seen in wind simulations by invoking differential wind recycling. In §4 we look at the scaling relation between SFR and  $M_*$  and its evolution to high- $z$ , emphasizing its connection with the matter accretion rate into halos. In §5 we further break down these trends in terms of centrals vs. satellite galaxies, and raise some issues regarding observed dwarf galaxies that none of the models reproduce. Finally, we summarise and discuss the broader implications of our work in §6.

## 2 SIMULATIONS

### 2.1 Code

Our simulations are run with an extended version of the GADGET-2 N-body + Smoothed Particle Hydrodynamic (SPH) code (Springel 2005, OD08). We assume a  $\Lambda$ CDM cosmology using the cosmological parameters based on recent WMAP results (Hinshaw et al. 2009):  $\Omega_M = 0.28$ ,

$\Omega_\Lambda = 0.72$ ,  $h \equiv H_0/(100 \text{ km s}^{-1} \text{ Mpc}^{-1}) = 0.7$ , a primordial power spectrum index  $n = 0.95$ , an amplitude of the mass fluctuations scaled to  $\sigma_8 = 0.82$ , and  $\Omega_b = 0.046$ . We refer to these runs as the r-series, where our general naming convention for a simulation run is `r[boxsize]n[particles/side][wind model]`. Our primary runs use the boxsize of  $48h^{-1}\text{Mpc}$  on a side with  $384^3$  dark matter and  $384^3$  gas particles. To expand our dynamic range we also run two additional sets of simulations that are identical except that they have box sizes of  $24h^{-1}\text{Mpc}$  and  $48h^{-1}\text{Mpc}$ , and have only  $256^3$  particles of each species. The particle masses and gravitational softening lengths are listed in Table 1.

An overview of the GADGET-2 code can be found in §2 of K09a. Additions to the public version of the code include cooling processes using the primordial abundances as described in Katz et al. (1996) and metal-line cooling as described in Oppenheimer & Davé (2006). Star formation is modeled using a subgrid recipe introduced in Springel & Hernquist (2003) where a gas particle above a critical density is modeled as a fraction of cold clouds embedded in a warm ionised medium following McKee & Ostriker (1977). Star formation (SF) follows a Schmidt law (Schmidt 1959) with the SF timescale scaled to match the  $z = 0$  Kennicutt law (Kennicutt 1998a). The density threshold for SF is  $n_H = 0.13 \text{ cm}^{-3}$ . We use a Chabrier (2003) initial mass function (IMF) throughout. The fraction of mass of the IMF going into massive stars, defined here as  $\geq 10 M_\odot$  and assumed to result in Type II supernovae (SNe), is  $f_{\text{SN}} = 0.18$ ; for reference, a Salpeter IMF has  $f_{\text{SN}} = 0.10$ .

Our simulations directly account for metal enrichment from sources including Type II supernovae (SNe), Type Ia SNe, and asymptotic giant branch (AGB) stars. Gas particles eligible for SF undergo self-enrichment from Type II SNe using the instantaneous recycling approximation, where mass, energy, and metallicity are assumed to immediately return to the ISM. Type II SN metal enrichment uses the metallicity-dependent yields calculated from the Chieffi & Limongi (2004) SNe models. Our prescriptions for feedback, described below, also assume the instantaneous input of energy from O and B stars (i.e. stars that are part of  $f_{\text{SN}}$ ). We input the Type Ia SNe rates of Scannapieco & Bildsten (2005), where an instantaneous component is tied to the SFR, and a delayed component is proportional to the stellar mass as described in OD08. Each Type Ia SN adds  $10^{51}$  ergs of thermal energy and the calculated metal yields of Thielemann et al. (1986) to surrounding gas; the mass returned is small compared to that from Type II SNe. AGB stellar enrichment occurs on delayed timescales from 30 Myrs to 14 Gyr, using a star particle's age and metallicity to calculate mass loss rates and metallicity yields as described in OD08. AGB mass and metal loss is returned to the three nearest surrounding gas particles. OD08 showed that the largest effect of AGB stars is to replenish the ISM, because a star particle can lose over 30% of its mass over  $t_H$ , nearly double the  $1 - f_{\text{SN}} = 18\%$  that is recycled instantaneously via Type II SNe.

Galactic outflows are implemented using a Monte Carlo approach analogous to star formation. Outflows are directly tied to the SFR, using the relation  $\dot{M}_{\text{wind}} = \eta \dot{M}_{\text{SF}}$ , where  $\eta$  is the *mass loading factor*. The probabilities for a gas particle to spawn a star particle is calculated as described above, and the probability to be launched in a wind is  $\eta$  times that.

If the particle is selected to be launched, it is given an additional velocity of  $v_w$  in the direction of  $\mathbf{v} \times \mathbf{a}$ , where  $\mathbf{v}$  and  $\mathbf{a}$  are the particle’s instantaneous velocity and acceleration, respectively; this would create a bipolar outflow for a thin disk, but in practice the outflow has a much larger opening angle. This subgrid model circumvents our inability to resolve the detailed physics of the ISM that generates winds, at the cost of introducing additional parameters. Choices of the parameters  $\eta$  and  $v_w$  define the “wind model”.

Once a gas particle is launched, its hydrodynamic (not gravitational) forces are turned off until either  $1.95 \times 10^{10} / (v_w \text{ (km s}^{-1}\text{)})$  years have passed or, more often, the gas particle has reached 10% of the SF critical density. This is intended to simulate the formation of hot chimneys extending out of a disk galaxy providing a low resistance avenue for outflows to escape into the IGM, which the spherically-averaged SPH algorithm at our current resolution is incapable of resolving. However, explicit decoupling neglects energy losses owing to the initial creation of such channels as well as any drag along their interfaces, and as such cannot drive turbulence in the ISM. We note that decoupling has a significant impact on wind propagation; simulations without such decoupling explored e.g. by Dalla Vecchia & Schaye (2008) show that decoupling greatly enhances the ability of material to escape a galaxy’s ISM. Hence decoupling must be regarded as an integral part of the wind models described in this work, having a significant impact on the results, particularly those associated with recycling of wind material (which would be much more prevalent if the hydrodynamic forces were never turned off). Springel & Hernquist (2003b) demonstrated that this decoupling achieves resolution convergence in the cosmic star formation history. We will later explicitly demonstrate resolution convergence for many of the galaxy properties of interest here.

## 2.2 Wind Models

For this paper we run four wind models, described as follows:

**No winds (nw):** We turn off our galactic winds. Note that, as with all simulations, energy is imparted thermally to ISM SPH particles using the Springel & Hernquist (2003) subgrid two-phase recipe where all SN energy is instantaneously coupled to the ISM. Owing to the explicit coupling of the hot and cold ISM phases, such energy cannot drive a wind.

**Constant winds (cw):** Feedback energy is added kinetically to gas particles at a constant rate relative to the SFR, with  $\eta = 2$  and a constant velocity  $v_w = 680 \text{ km s}^{-1}$ . This is intended to mimic the constant-wind model of Springel & Hernquist (2003), but with some notable differences. Here  $\eta$  is defined relative to the SFR of the entire Chabrier IMF, and not just the long-lived stars in a Salpeter IMF as it is defined by Springel & Hernquist (2003). Second,  $v_w = 680 \text{ km s}^{-1}$  is used rather than  $484 \text{ km s}^{-1}$ , because there is more SN energy per mass formed in a Chabrier IMF. The kinetic energy imparted to wind particles per unit SF is  $9.25 \times 10^{48} \text{ erg} / M_\odot$ , which is 95% of the SN energy in this IMF assuming all stars  $\geq 10 M_\odot$  add  $10^{51} \text{ ergs/SN}$ . The hydrodynamic decoupling time in this model has a maximum of  $2.9 \times 10^7$  years. We note that this model is similar to the “REFERENCE” outflow model of the OverWhelmingly Large Simulations (OWLS Schaye et al. 2010), except

that we include hydrodynamic decoupling while they do not; in fact, they have also considered models likw nw and vzw (below) except without decoupling.

**Slow winds (sw):** We run an alternative constant-wind model with the only difference being the outflow velocities are half as high as the cw winds (i.e.  $v_w = 340 \text{ km s}^{-1}$  and  $\eta = 2$ ). Therefore only roughly a quarter of the SN energy couples kinetically into these outflows.

### Momentum-conserved winds (vzw):

This model uses the analytic derivations by Murray, Quataert, & Thompson (2005) based on the galaxy velocity dispersion ( $\sigma$ ). Its implementation is explained in Oppenheimer & Davé (2006) and updated in OD08 with the addition of an *in situ* group finder to calculate  $\sigma$  using galaxy mass following Mo, Mao, & White (1998). The wind parameters vary between galaxies using the following relations:

$$v_w = 3\sigma\sqrt{f_L - 1}, \quad (1)$$

$$\eta = \frac{\sigma_0}{\sigma}, \quad (2)$$

where  $f_L$  is the luminosity factor in units of the galactic Eddington luminosity (i.e. the critical luminosity necessary to expel gas from the galaxy potential), and  $\sigma_0$  is the normalization of the mass loading factor. Here we randomly select  $f_L = [1.05, 2]$  for each SPH particle, following observations by Rupke, Veilleux & Sanders (2005), and include a metallicity dependence for  $f_L$  owing to more UV photons output by lower metallicity stellar populations

$$f_L = f_{L,\odot} \times 10^{-0.0029 * (\log Z + 9)^{2.5} + 0.417694}. \quad (3)$$

We further add an extra kick to get out of the potential of the galaxy in order to simulate continuous pumping of winds until it is far from the galaxy disk (as argued by MQT05). These parameters  $v_w$  and  $f_L$  are well-constrained by observations, leaving the only unconstrained free parameter as  $\sigma_0$ . We set  $\sigma_0 = 150 \text{ km s}^{-1}$ , which is the same efficiency factor of the mass loading used in OD08. The energy budget for winds scales as  $\propto \eta v_w^2 \propto \sigma$ , and exceeds the supernova energy budget only at quite large halo masses of  $\gtrsim 10^{14} M_\odot$  (at  $z = 0$ ). Since we do not include any type of feedback that quenches star formation in massive galaxies (Gabor et al. 2010), our simulations do not accurately model these systems in any case. In general, the wind energetics in this model are quite modest, and despite the large mass outflow rates and speeds around the escape velocity, are generally well below the supernova energy budget (globally, about half in the r48n384vzw run). This does not even account for radiative energy input from massive stars, which can exceed the energy output from supernovae.

These wind models allow us to illustrate how outflows impact the scaling relations of galaxies. An important difference comes from the wind speed scaling: In the momentum-conserved outflows case, the wind speed is typically around the galaxy escape velocity, and scales with it. Hence in this model, the potential well of the galaxy does not play a governing role in wind dynamics as a function of mass. This stands in contrast to the canonical model for outflows (e.g. Dekel & Silk 1986) in which outflows escape from small galaxies owing to their small potential wells while being recaptured in large galaxies. If gravity was the only relevant force, this model should show ex-

**Table 1.** Simulation runs

Name	$L^a$	$\epsilon^b$	$m_{\text{SPH}}$	$m_{\text{dark}}$	$m_{\text{gal}}^c$	$v_w$ ( km s $^{-1}$ )	$\eta^d$	$E_{\text{wind}}/E_{\text{SN}}^e$	$p_{\text{wind}}/p_*^f$	$f_*^g$	$f_{\text{wind}}^h$
r48n384nw	48	2.5	$3.6 \times 10^7$	$1.8 \times 10^8$	$\sim 10^{10}$	0	0	0	0	0.220	0
r48n384vzw	48	2.5	$3.6 \times 10^7$	$1.8 \times 10^8$	$1.1 \times 10^9$	$\propto \sigma$	$\propto \sigma^{-1}$	0.49 <sup>i</sup>	5.2	0.097	0.345
r48n384cw	48	2.5	$3.6 \times 10^7$	$1.8 \times 10^8$	$1.1 \times 10^9$	680	2	0.95	8.7	0.045	0.174
r48n384sw	48	2.5	$3.6 \times 10^7$	$1.8 \times 10^8$	$1.1 \times 10^9$	340	2	0.24	4.4	0.124	0.476
r24n256nw <sup>j</sup>	24	1.875	$1.5 \times 10^7$	$7.6 \times 10^7$	$\sim 4 \times 10^9$	0	0	0	0	-	0
r24n256vzw <sup>j</sup>	24	1.875	$1.5 \times 10^7$	$7.6 \times 10^7$	$4.7 \times 10^8$	$\propto \sigma$	$\propto \sigma^{-1}$	-	-	-	-
r24n256cw <sup>j</sup>	24	1.875	$1.5 \times 10^7$	$7.6 \times 10^7$	$4.7 \times 10^8$	680	2	0.95	8.7	-	-
r24n256sw <sup>j</sup>	24	1.875	$1.5 \times 10^7$	$7.6 \times 10^7$	$4.7 \times 10^8$	340	2	0.24	4.4	-	-
r48n256nw	48	3.75	$1.2 \times 10^8$	$6.1 \times 10^8$	$\sim 3 \times 10^{10}$	0	0	0	0	0.182	0
r48n256vzw	48	3.75	$1.2 \times 10^8$	$6.1 \times 10^8$	$3.7 \times 10^9$	$\propto \sigma$	$\propto \sigma^{-1}$	0.52 <sup>i</sup>	5.1	0.081	0.257
r48n256cw	48	3.75	$1.2 \times 10^8$	$6.1 \times 10^8$	$3.7 \times 10^9$	680	2	0.95	8.7	0.046	0.179
r48n256sw	48	3.75	$1.2 \times 10^8$	$6.1 \times 10^8$	$3.7 \times 10^9$	340	2	0.24	4.4	0.116	0.448

<sup>a</sup> Box size in comoving  $h^{-1}\text{Mpc}$ .<sup>b</sup> Gravitational softening length in comoving  $h^{-1}\text{kpc}$  (equivalent Plummer).<sup>c</sup> Galaxy mass resolution limit in  $M_{\odot}$ ; see discussion in §3.1 of no-wind case.<sup>d</sup>  $\eta \equiv \dot{M}_{\text{wind}}/\text{SFR}$ .<sup>e</sup> Total feedback energy divided by SN energy (Chabrier IMF).<sup>f</sup> Total feedback momentum divided by momentum output by  $10^7$  yr old stellar population (Chabrier IMF).<sup>g</sup> Global mass fraction of baryons in stars at  $z = 0$ .<sup>h</sup> Global mass fraction of baryons that have been ejected in winds by  $z = 0$ .<sup>i</sup> Volume-averaged to  $z = 0$ ; in this model it is  $\propto \sigma$ .<sup>j</sup> Owing to a hardware failure, we only have information at  $z=0,1,3$  for these runs.

actly the same escape fraction of outflowing material from galaxies of all masses. In actuality, hydrodynamic slowing plays an important role (Oppenheimer & Davé 2008), and because more massive galaxies live in denser gaseous environments, this retards winds more around more massive galaxies, causing greater return of wind material to these systems (Oppenheimer et al. 2010).

The constant- $\eta$  models (sw and cw) behave more like the canonical model for winds, in the sense that at low galaxy masses their (constant-velocity) winds can escape the potential well, while at high masses they cannot. One can envision this as an “effective” mass loading factor that is roughly the input value of 2 at small masses, but drops to zero at large masses (Finlator & Davé 2008). Alternatively, one can view this as rapid recycling of wind material back into galaxies at high masses (Oppenheimer et al. 2010). In any case, the constant wind speed imparts a feature at a mass scale corresponding to where the assumed wind velocity is comparable to the galaxy escape velocity. Because of the different wind speeds in cw and sw, this feature should occur at different masses (roughly a factor of eight apart in halo mass, given the factor of two difference in wind speeds). Hence comparing these two models enables us to identify features in scaling relations that are related to how the effective mass loading factor scales with mass; this is discussed extensively in Oppenheimer et al. (2010, see e.g. their Figure 4). As we will argue later, it is the scaling of the (effective) mass loading factor with  $M_*$  that primarily governs most galaxy scaling relations.

Our twelve runs are listed in Table 1. They were run at the University of Arizona’s SGI cluster, ICE, the National Center for Supercomputing Applications’ Intel cluster, Abe, and the University of Massachusetts’ Xeon cluster, Eagle. Each run took between 100,000 and 150,000 CPU hours, al-

though nearly 1 million CPU hours were used when including smaller box sizes and various test runs. We note that due to technical difficulties, we only have galaxy catalogs for the r24 runs at  $z = 0, 1, 3$ , and do not have any information regarding satellite galaxies in these runs. However, all the important trends can be seen from the other runs at the redshifts where the r24 runs are not available.

We emphasize that all these models are heuristic and intended only to explore how these wind scalings impact galaxy properties. We are not directly advocating any particular physical process, though we are attempting to use physically-motivated recipes. In particular, the momentum-driven wind scalings can arise from models that only employ supernova energy to drive winds, owing to the interactions of super-heated ISM material with surrounding gas (e.g. Dalla Vecchia & Schaye 2008). Hence the name “momentum-driven” is only intended to indicate the scalings rather than a detailed physical model.

Nevertheless, owing to its prominence in this paper and others, we briefly discuss some issues related to the physics of the momentum-driven scalings wind model. The basic physical motivation is a model in which radiation pressure drives dust outwards, which couples to the gas to generate an outflow (Murray, Quataert, & Thompson 2005; Zhang & Thompson 2010). First, it is important to note that the momentum input required to drive winds at hundreds of km/s with mass loading factors as assumed above significantly exceeds the photon momentum emitted by the stellar populations (M. Haas & J. Schaye, priv. comm. Haas 2010). We show this ratio in Table 1, and is a factor of 5.2 for our r48n384vzw simulation<sup>1</sup>. Following Haas (2010), this is

<sup>1</sup> The momentum requirements are similarly large for the

calculated from the luminosity of stars for a solar-metallicity  $10^7$  yr old stellar population assuming a Chabrier (2003) IMF, divided by  $c$ . The large value indicates that momentum alone, under the assumption of single photon scattering, cannot power the outflows in the vzw model.

It is possible that subsequent re-radiation of photons could cause significantly more momentum deposition than what is emitted by the stars if the gas is optically thick to infrared radiation. For an infrared optical depth of  $\tau_{IR}$ , momentum deposition is increased by  $1 + \tau_{IR}$ . This factor can only be significantly greater than unity in highly dense gas where young stars form. Hopkins, Quataert, & Murray (2011) computed  $\tau_{IR}$  in simulations of radiation-driven winds from high-resolution disk galaxies, and indeed found that in some cases  $\tau_{IR}$  can approach an order of magnitude, driving an outflow velocity of  $\sim 200$  km/s leaving the disk with mass loading factors of order unity. While this is encouraging, the issue of whether enough momentum is available from stars, and whether it can effectively couple to the dust and in turn to the gas, remains an open question.

Another possibility is that supernovae and photons from young stars work together to drive winds (e.g. Nath & Silk 2009; Murray, Ménard, & Thompson 2010). Invariably, this must be happening at some level, since both processes are energetically comparable. Haas (2010, Figure 2.19) showed that the momentum from SNe can be an order of magnitude larger than that from stellar radiation at  $10^7$  yr after the burst, although it drops rapidly with time. Murray, Ménard, & Thompson (2010) showed that for a 300 km/s wind, radiation pressure can yield a mass loading factor up to  $\eta = 0.4$  in the single-scattering regime, which is factors of many less than what our momentum-driven wind scalings require. Hence supernova momentum input would have to dominate overall, particularly at large radii where the optical depth to absorb photons becomes small. Despite being driven primarily by supernovae and not radiation pressure, the scalings predicted in this scenario continue to follow those expected for momentum-driven winds (Murray, Ménard, & Thompson 2010).

In short, the momentum-driven wind scalings that we have assumed challenge the available momentum budget, but could plausibly arise from a combination of physical processes. Much work remains to be done to marry large-scale constraints from cosmological simulations with detailed studies of wind expulsion from star-forming regions.

### 2.3 Galaxy and halo identification

We use SKID<sup>2</sup> (Spline Kernel Interpolative Denmax) to identify galaxies as bound groups of star-forming gas and stars (Kereš et al. 2005; Oppenheimer et al. 2010). Since we specifically include just star-forming gas, our simulated galaxies only account for gas within the galactic ISM and not from the extended halo; this defines the galaxy’s gas mass. Our galaxy stellar mass limit is set to be  $\geq 64$  star particles (Finlator et al. 2006), resulting in the masses listed under  $m_{\text{gal}}$  in Table 1. We will argue that for the no-wind case

the resolution convergence is poorer, and we list approximate masses that show convergence. Unless otherwise noted, we will only consider galaxies with stellar mass  $M_* \geq m_{\text{gal}}$  in our analysis.

We separate galaxies into central and satellite galaxies by associating each galaxy with a halo. We identify halos via a spherical overdensity algorithm (Kereš et al. 2005). In brief, we begin at the center of each galaxy and expand out spherically until the mean density enclosed equals that of a virialized halo (Kitayama & Suto 1996). We then subsume all galaxies whose centers are within that of a larger galaxy’s halo into that larger halo. In this way, each galaxy is a member of one and only one halo. The central galaxy is the largest one that is at the center of the halo, and any other galaxies within that halo are satellites.

## 3 STELLAR MASS AND STAR FORMATION RATE FUNCTIONS

### 3.1 Stellar Mass Function

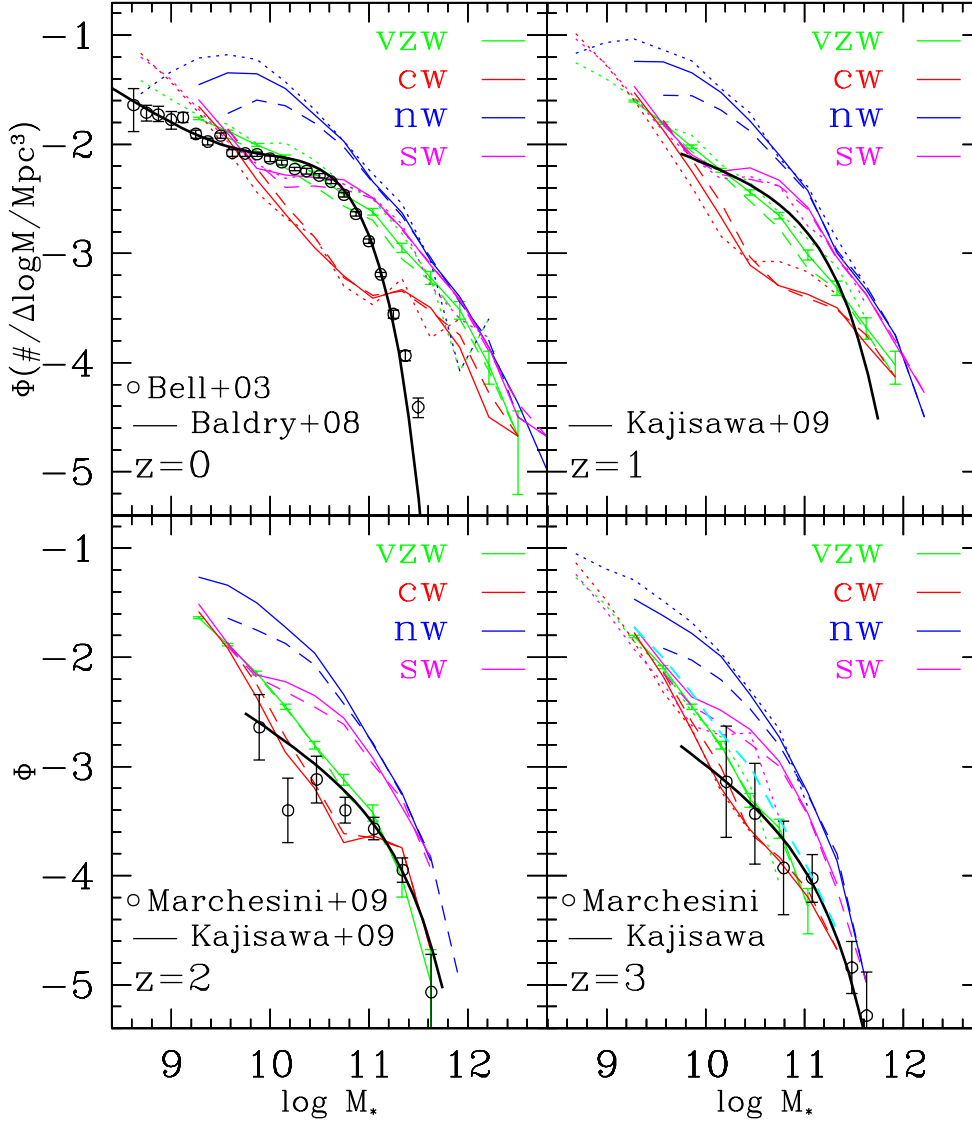
We begin by considering the stellar mass function and its evolution in our simulations. Stellar mass appears to be a governing parameter for galaxy properties, having fairly tight scaling relations with many other fundamental galaxy properties, relatively independently of environment (e.g. Li et al. 2010). Hence the stellar mass function provides a key barometer for simulated galaxy populations.

Figure 1 shows the galaxy stellar mass function (GSMF) out to  $z = 3$  in our four outflow simulations. Data is shown for comparison from Bell et al. (2003,  $z \sim 0$ , points), Baldry, Glazebrook, & Driver (2008,  $z \sim 0$ , curve), Kajisawa et al. (2009,  $z = 1, 2, 3$ , curves), and Marchesini et al. (2009,  $z = 2, 3$ , curves). These were selected as fairly recent determinations of the stellar mass function from some of the deepest available near-infrared observations, though it is far from a complete sample of available data. The curves represent Schechter function best fits, while the data points (from different samples) give an indication of the uncertainties. Note that the Kajisawa et al. (2009) data plotted at  $z = 1$  is actually centered at  $z \approx 0.75$ , but the evolution is not rapid during this period. Also, we have scaled all data to a Chabrier (2003) IMF (as assumed in the simulations), by dividing the stellar masses by 1.25 for those quoted using a *diet* Salpeter IMF (namely, Bell et al. 2003; Baldry, Glazebrook, & Driver 2008), and by 1.8 for those quoted using a Salpeter IMF (Kajisawa et al. 2009). Marchesini et al. (2009) used a Kroupa (2001) IMF which is very similar to Chabrier, so we apply no IMF correction. Finally, the Bell et al. (2003) data has been corrected to  $h = 0.7$ ; all other data shown assumed this value for the Hubble constant.

A test of numerical resolution convergence is provided by comparing the solid, dotted, and dashed lines for each model, which are from the r48n384, r24n256, and r48n256 series of runs, respectively. The difference in mass resolution between r48n384 and r48n256 is a factor of 2.4, while between r48n384 and r24n256 it is 3.3; without accounting for this, convergence will appear slightly better at low resolution. In actuality, for the wind models at every redshift the GSMFs show very good convergence (modulo some stochastic fluctuations at the massive end), and the faint end of

constant- $v_w$  models, but in this case the physical motivation is supernova energy, so the momentum input is not relevant.

<sup>2</sup> <http://www-hpcc.astro.washington.edu/tools/skid.html>



**Figure 1.** Stellar mass functions at  $z = 0, 1, 2, 3$  in cosmological hydrodynamic simulations employing our four galactic outflow scalings: momentum-conserved winds (green), constant winds (red), no winds (blue), and slow winds (magenta). Solid lines show results from the r48n384 series of runs, dotted lines show r24n256 series, and dashed lines show r48n256 series; these illustrate resolution convergence, although when interpreting convergence one should keep in mind that these runs are not equally (logarithmically) spaced in mass resolution: r48n256 is  $2.4\times$  r48n384, which is  $3.3\times$  r24n256. The momentum-conserved wind case shows Poisson error bars as a representative example. Cyan dashed curve at  $z = 3$  shows the result of adding a Gaussian random scatter of  $\sigma = 0.3$  dex to each galaxy’s stellar mass in the momentum-conserved wind case. Data points at  $z = 0$  from Bell et al. (2003), curve at  $z = 0$  from Baldry, Glazebrook, & Driver (2008), curves at  $z = 1, 2, 3$  from Kajisawa et al. (2009), and data points at  $z = 2, 3$  from Marchesini et al. (2009).

the higher-resolution run joins smoothly onto that of the larger-volume run. For the no-wind simulations, this is not the case: The higher-resolution run deviates from the lower-resolution run at a  $M_*$  that is much larger than the nominal 64 star particle galaxy mass resolution. The reason can be traced back to resolution convergence for halos, as opposed to galaxies: Halos also require approximately 64 particles to robustly host galaxies, and in the no-wind case this corresponds to a much higher  $M_*$  than in the wind models where star formation at a given halo mass is much suppressed (Oppenheimer et al. 2010). Hence convergence for the no-wind case differs from the wind runs, and its resolved galaxy mass is higher by roughly an order of magnitude (as

indicated in Table 1). The low-mass peak of the GSMF is shifted over by roughly the difference in mass resolution between the two models, further indicating that the GSMF here is impacted by resolution effects. Hence the turn-down in the no-wind GSMF at low masses is a numerical artifact, not a prediction. For the wind models, this turn-down happens below the nominal stellar mass resolution.

The no-wind case (nw; blue), where resolution-converged, shows the classic behavior that the GSMF well exceeds observations at all masses (see e.g. Kereš et al. 2009b, for a more detailed discussion). This is symptomatic of the overcooling problem (White & Frenk 1991; Balogh et al. 2001; Davé et al. 2001), in which there are

too many baryons locked in stars at all epochs without strong feedback. We note that this occurs at *all* redshifts and masses back to  $z \sim 4$  (and even farther back; see Davé, Finlator, & Oppenheimer 2006), indicating that the overcooling problem is not just a late-time phenomenon and must be mitigated in the early Universe.

It has long been suggested that galactic outflows could suppress star formation to solve the overcooling problem. The magnitude of suppression, factors of several even at maximum galaxy formation efficiency around  $M^*$  increasing to much larger factors at larger and smaller masses, indicates that outflows must eject a substantial amount of gas from galaxies and/or suppress accretion by adding energy to the surrounding IGM. In star-forming galaxies (typically  $M_* \lesssim M^*$ ), the dominant energy source is star formation, either from supernovae or young stars. This motivates all of our wind models having mass loading factors exceeding unity. For concreteness, Table 1 shows as its final two columns the global mass fraction of baryons in stars at  $z = 0$  and ejected in winds by  $z = 0$ , respectively. For the momentum-conserved run, the ratio between the two is roughly 3.5, i.e.  $3.5\times$  more baryons have been ejected from galaxies than have formed into stars by  $z = 0$ . The constant- $\eta$  models have a ratio of approximately 3.8. That this ratio significantly exceeds unity is a generic feature of all models that solve overcooling via an ejective feedback mechanism such as galactic outflows.

The exact shape of the  $z = 0$  GSMF depends sensitively on outflows, albeit in a subtle way. As discussed in Oppenheimer et al. (2010), it is not the overall suppression by ejection that governs the shape, but rather the effectiveness of subsequent re-accretion of ejected material, i.e. recycled wind mode accretion. As shown in Oppenheimer et al. (2010), without wind recycling, all GSMFs look fairly similar, and show a steep power law behavior with a faint-end slope comparable to that of the halo mass function. Because wind material re-accretes into larger galaxies faster (“differential recycling”), it boosts high-mass galaxy masses relative to low-mass ones, and therefore flattens the faint end of the stellar mass function. At sufficiently small masses, the timescale for wind re-accretion exceeds the Hubble time, at which point the mass function returns towards tracking the dark matter halo mass function as there is no differential effect from recycling. At sufficiently large masses, recycling is so fast that it effectively is like having no winds at all. This creates a three-tier behavior for the GSMF in simulations: It follows the steep dark matter mass function both above and below the mass range where differential recycling operates, and it is flatter within that mass range.

All our wind models display this three-tiered behavior, though it is less evident in some cases. At high masses, they have a slope similar to that of the no-wind model. In the intermediate mass regime, the slope is flatter or even inverted, and finally at low masses once again the GSMF is reverts to being steep. We note that all models grossly overpredict the massive end of the GSMF compared to observations. This is because we do not have any feedback mechanism to truncate star formation in massive galaxies, such as feedback from active galactic nuclei (AGN; e.g. Di Matteo et al. 2005). Hence our first key point is that our current simulations can only reliably probe the regime of star-forming galaxies, which dominate at masses  $\lesssim M^* \approx 10^{11} M_\odot$  (Salim et al. 2007).

In Gabor et al. (2010) we show that it is possible to include empirical feedback mechanisms to quench star formation in massive galaxies, without significantly affecting the population of galaxies below  $M^*$ . This is consistent with the observation that strong AGN activity is not seen in lower-mass galaxies today ( $M_* \lesssim 10^{10.5} M_\odot$ ; Kauffmann et al. 2004).

The exact transitions between the various GSMF tiers depend strongly on wind model. In the constant- $\eta$  cases, the three-tiered behavior is manifested as a bump in the GSMF at high masses at  $z = 0$ . In the constant wind case (cw; red), the middle tier covers a small mass range, and differential recycling is so strong that it actually produces an inverted slope of the GSMF within that small mass range. Outside that, the GSMF is quite steep, roughly following the slope of the no-wind case. The slow-wind case (sw; magenta) follows a similar pattern, but the mass scale of the differential recycling is lower because wind speeds are slower, and hence wind recycling becomes effective at a smaller scale. In neither case does the GSMF resemble the observed one at  $z = 0$  even in the regime where quenching feedback is unimportant, although the slow-wind case is not as far off.

The momentum-driven scalings case (vzw; green) produces a more gradual differential recycling curve than the constant- $\eta$  cases (Oppenheimer et al. 2010). Hence the middle tier is not inverted, but merely shallower than the high and low mass ends of the GSMF. This mimics the behavior exhibited by the observed GSMF. Recent observations by Baldry, Glazebrook, & Driver (2008) have conclusively detected an upturn to a steep faint-end slope. In detail, the vzw simulation is still mildly steeper than observed and the upturn occurs at slightly too high a mass. If our physical interpretation for the origin of the GSMF is correct, this would imply that the momentum-conserved wind model has a differential recycling curve that is close to, but not quite, correct. It is worth mentioning that modeling the dynamics of wind recycling is subject to significant numerical difficulties as discussed in Oppenheimer et al. (2010, though more so at in higher-mass halos where hot gas is present), so the level of discrepancy with data is probably within modeling uncertainties, but more careful simulations are needed to determine this.

The evolution of the GSMF can now be probed to high redshifts thanks to advancing deep near-IR surveys. At the massive end, the observed GSMF has a less pronounced cut-off at high- $z$ . Since this truncation is associated with the presence of “red and dead” galaxies, the relative dearth of such galaxies at  $z \gtrsim 2$  explains why the truncation is much less sharp. At  $z \sim 2 - 3$ , the vzw run yields a GSMF at  $M_* \gtrsim 10^{10.5} M_\odot$  that is in fair agreement with data, although it appears somewhat too steep. Meanwhile, sw overproduces the number of galaxies at these stellar masses similar to the no-wind case. The constant wind case generally matches well here, although it still shows a bump at  $M_* \gtrsim 10^{11} M_\odot$  that is not seen in the data. Considering all redshift from  $z = 0 - 3$  in toto, the momentum-driven scalings model yields the best match from amongst these models to the population of star-forming galaxies at  $10^{10} \lesssim M_* \lesssim 10^{11} M_\odot$ .

The faint-end slope of the GSMF has been observed to evolve towards being steeper at high redshifts. Our simulations follow this trend qualitatively, but only within the intermediate mass regime where differential recycling flat-



tens (or inverts) the GSMF slope at later times. Outside of this regime, the slope always approaches the faint-end halo mass slope of  $\alpha \approx 2$ . For instance, in the vzw run, the intermediate mass regime occurs at  $10^{9.7} \lesssim M_* \lesssim 10^{10.7} M_\odot$ , and the slope at  $z = 0$  is  $\alpha \approx 1.4$ , which is close to the observed slope in that mass range. In the sw case, the intermediate mass regime is narrower,  $10^{10} \lesssim M_* \lesssim 10^{10.5} M_\odot$ , while in the cw case it is equally narrow but occurs at a mass  $\sim 8\times$  higher. In both constant- $\eta$  simulations, the GSMF slope at  $z = 0$  is inverted in this regime, i.e.  $\alpha < 1$ , but at higher redshifts  $\alpha$  increases.

The general reason for the increase in  $\alpha$  within the intermediate mass regime is that wind recycling becomes less important at higher redshifts. This is primarily because there is less time for ejected material to return to galaxies (Oppenheimer et al. 2010). Our simulations, particularly the momentum-conserved case, tend to find median recycling times that are fairly constant at  $\sim 1 - 2$  Gyr, independent of cosmic epoch (Oppenheimer & Davé 2008); this is partly because wind speeds at a given  $M_*$  are higher (Oppenheimer & Davé 2008) at high- $z$ . Hence the features associated with recycling become less prominent, and in fact they are essentially invisible at  $z \gtrsim 2$  in the vzw case.

Observationally,  $\alpha$  is seen to evolve as  $\alpha \approx \alpha_0 + (0.082 \pm 0.033)z$  (Fontana et al. 2006), where  $\alpha_0 \approx 1.2 - 1.3$ . Effectively, this corresponds to the slope in the mass regime of  $10^{10} \lesssim M_* \lesssim 10^{11} M_\odot$ , which is what can be probed in practice out to high- $z$  at this time; at lower masses, the present-day GSMF becomes steeper, but this cannot be reliably traced at high- $z$ . The momentum-driven scalings model matches well at low- $z$  (below  $M^*$ ), but at high- $z$  the faint end is quite a bit steeper: e.g. at  $z = 2$ ,  $\alpha \approx 2$  in the regime where it is observed to be more like 1.5 or so. Hence while the evolutionary trend is qualitatively as observed, there are quantitative discrepancies in the sense that this model has too many small galaxies (as is the case with all models). This has also been noted at  $z \sim 4 - 7$  in a comparison of various simulations to mass function observations (González et al. 2011); all models have too steep a mass function at  $M_* \lesssim 10^9 M_\odot$ . This may indicate that feedback processes in very small systems are not being correctly represented in these models, a point that will be reiterated throughout this paper.

One issue that may explain part of the difference between the simulations and data are observational uncertainties in determinations of stellar masses, which can become significant particularly at high- $z$ . To explore this, at  $z = 3$  we added a Gaussian random scatter with  $\sigma = 0.3$  dex to each galaxy's stellar mass in the momentum-conserved wind simulation (which is a typical observational uncertainty; see Marchesini et al. 2009), and recomputed the stellar mass function. The result is shown as the dashed cyan line in Figure 1. Because the mass function is steep, more small galaxies get scattered to larger masses than vice versa, and the mass function does become slightly shallower (and in this case, agrees slightly better with observations at the massive end). But this does not go far towards reducing the overproduction of small galaxies in the simulations. There are, additionally, substantial systematic uncertainties in determining stellar masses from photometric data (e.g. Marchesini et al. 2009); we have not considered such effects here, but it's con-

ceivable that they could dominate over the statistical errors. Hence while this effect should be accounted for when comparing carefully to data, it does not qualitatively alter the faint end discrepancy.

Overall, the momentum-driven scalings model does the best job of the models considered in reproducing the observed GSMFs around  $M^*$  from  $z = 3 \rightarrow 0$ . There are still significant discrepancies at higher and lower masses, so the agreement is only good in the range of  $10^{10} \lesssim M_* \lesssim 10^{11} M_\odot$ . Nevertheless, this is a significant success, a first for cosmological hydrodynamic simulations (that we are aware of). While the discrepancy at high masses is well-known and strongly suggestive of quenching feedback absent in these simulations, the discrepancy at small masses is less certain owing to still substantial observational uncertainties at high- $z$ . Upcoming deeper observations should quantify this discrepancy to greater precision, possibly providing insights into the nature of feedback processes in high-redshift dwarf galaxies.

### 3.2 Star Formation Rate Function

Figure 2 shows the star formation rate function ( $\Phi_{\text{SFR}}$ ) for galaxies in our four wind models at four redshifts. The dotted line shows the SFR at the galaxy stellar mass limit listed in Table 1, obtained by fitting the relationship between SFR and  $M_*$  as displayed in Figure 3. Since we do not have a clean stellar mass threshold in this plot, we show all galaxies, but  $\Phi_{\text{SFR}}$  at SFRs below the dotted line may not be robust. Because the relationship between SFR and  $M_*$  varies slightly with wind model, each model has a different SFR threshold. Note that the no-wind case has a significantly higher resolved galaxy mass threshold in Table 1 for reasons described in the previous section, and hence its dotted line is at a much higher mass. Observations at  $z = 0$  from a GALEX+IRAS compilation by Martin et al. (2005) are shown as the solid black line, at  $z \sim 1$  from Ly et al. (2010), and at  $z = 2$  from an H $\alpha$  survey by Hayes, Schaerer, & Östlin (2010).

At  $z = 0$ ,  $\Phi_{\text{SFR}}$  shows different behaviors amongst the various wind models that mimic many features seen in the GSMF. The effect of differential recycling is seen in the three-tiered behavior of the constant- $\eta$  models, but the intermediate regime is not obviously seen in the vzw case. Nevertheless, relative to no-winds, vzw shifts star formation from smaller to larger systems, owing both to its mass loading dependence as well as differential recycling. The large amount of recycled wind accretion at late times (Oppenheimer et al. 2010) produces a  $\Phi_{\text{SFR}}$  at high masses that is actually higher for all the wind models than for the no-wind case. The winds are metal-enriched and so are particularly effective at cooling back onto the galaxy (often failing to shock heat to the temperature of surrounding halo gas despite their large outflow velocities), and they delay star formation towards later epochs making the effect at high masses stronger towards lower redshifts.

Moving to higher redshifts, the strength of the differential recycling features in the cw and sw simulations lessen as with the GSMF, but they are still prominent even at the highest redshifts. For vzw,  $\Phi_{\text{SFR}}$  becomes quite a bit steeper at high- $z$ . The shape of the no-wind  $\Phi_{\text{SFR}}$  does not vary, but the amplitude evolution of  $\Phi_{\text{SFR}}$  is fairly constant from  $z = 3 \rightarrow 2$ , and then drops with time reflecting the

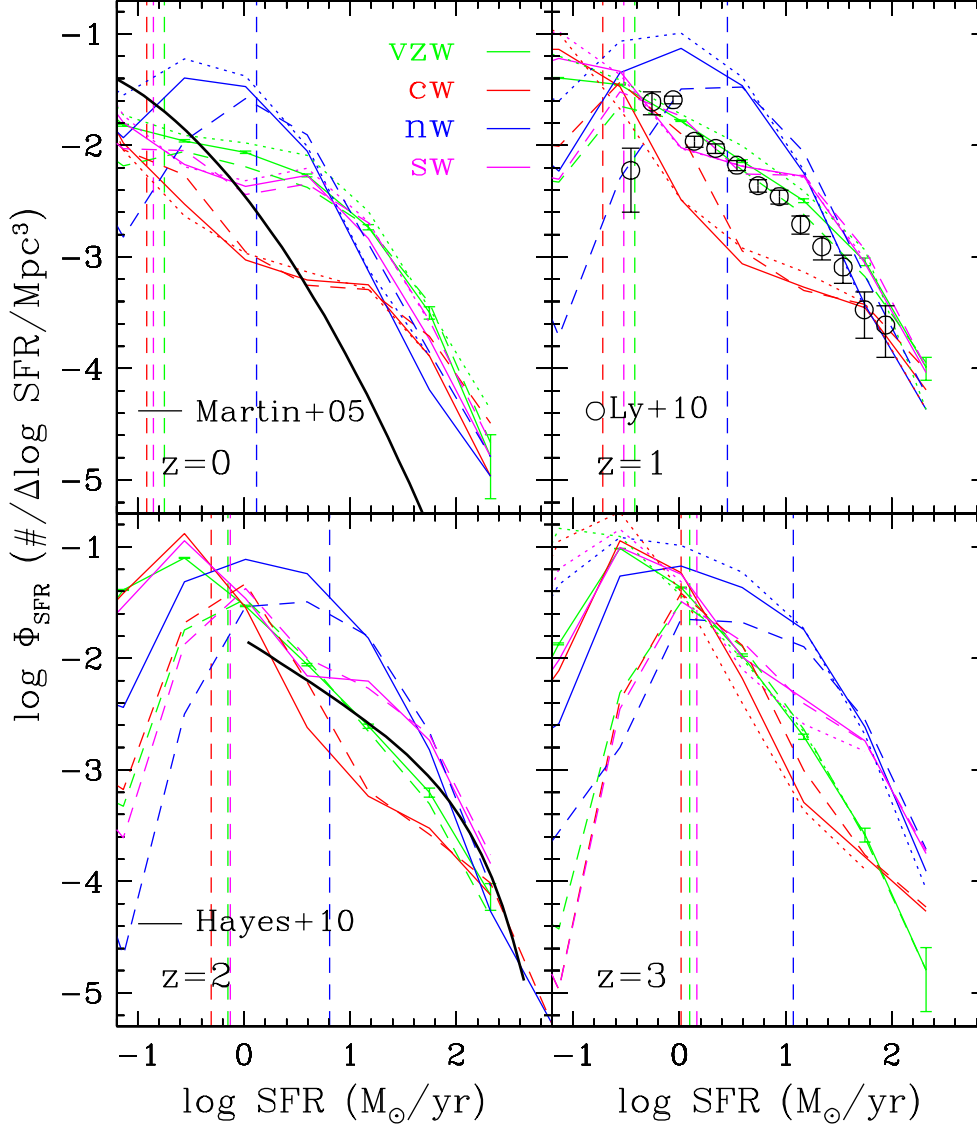


**Figure 2.** Star formation rate functions  $\Phi_{\text{SFR}}$  at  $z = 0, 1, 2, 3$  in our r48n384 series of simulations employing our four galactic outflow scalings: momentum-conserved winds (green), constant winds (red), no winds (blue), and slow winds (magenta). Solid lines show results from the r48n384 series of runs, dotted lines show r24n256 series ( $3.3\times$  better mass resolution), and dashed lines show r48n256 series ( $2.4\times$  worse mass resolution). The momentum-conserved case shows Poisson error bars as a representative example. Dotted lines indicate the SFR at galaxy stellar mass limit (see Table 1) at each redshift, from a linear fit to the  $M_*$ –SFR relation for each model; below this SFR, the results are less likely to be robust. The thick line at  $z = 0$  shows  $\Phi_{\text{SFR}}$  derived from ultraviolet plus infrared data from Martin et al. (2005), while points at  $z = 1$  and thick line at  $z = 2$  show  $\Phi_{\text{SFR}}$  derived from observed H $\alpha$  luminosity functions at  $z \approx 0.81$  by Ly et al. (2010) and at  $z \approx 2.2$  by Hayes, Schaerer, & Östlin (2010), respectively.

overall drop in cosmic SFR. For example,  $\Phi_{\text{SFR}}(10M_{\odot}/\text{yr})$  at  $z \sim 2 - 3$  is about  $\sim 10^{-1.5}$ , dropping to  $\sim 10^{-2}$  at  $z = 1$  and  $10^{-3}$  at  $z = 0$ . In contrast, the momentum-conserved wind model shows a less rapidly evolving  $\Phi_{\text{SFR}}$ , as  $\Phi_{\text{SFR}}(10M_{\odot}/\text{yr}) \approx -2.3$  at all redshifts, although  $\Phi_{\text{SFR}}$  shows a flatter faint-end slope at low redshifts.

Compared to observations at  $z = 0$  (Martin et al. 2005), none of the models fare well, as they all overproduce the number of star-forming galaxies at higher SFR’s. This is not surprising, and can be straightforwardly traced to the lack of any feedback mechanism to quench star formation in massive galaxies (Gabor et al. 2010) as observed in the real Universe (e.g. Kauffmann et al. 2004). Note that the

number of star-forming galaxies must be suppressed down to quite moderately star-forming systems. For instance, in the momentum-conserved case,  $\Phi_{\text{SFR}}$  is overproduced at  $\text{SFR} \gtrsim 1M_{\odot}/\text{yr}$ . Therefore galaxies larger than the Milky Way must be increasingly quenched, which coincides with the discrepancy in the GSMF above  $M^*$ . The star formation rate function therefore provides a strong constraint on models for quenching massive galaxies.

At higher redshifts, we compare to the H $\alpha$  luminosity function determined at  $z = 0.81$  by Ly et al. (2010) and at  $z \approx 2.2$  by Hayes, Schaerer, & Östlin (2010), both of which probe down to  $\sim 1M_{\odot}/\text{yr}$ . We obtain SFR from  $L_{\text{H}\alpha}$  using the Kennicutt (1998b) conversion divided by 1.8

to correct from Salpeter to Chabrier IMF, namely  $\text{SFR} = 4.4 \times 10^{-42} L_{H\alpha} M_\odot/\text{yr}$ . For Ly et al. (2010) we show their extinction- and incompleteness-corrected  $2.5\sigma$  sample. For Hayes, Schaerer, & Östlin (2010) we show their “combined” best-fit Schechter function which is supplemented by bright-end data from Geach et al. (2008), and correct for 0.977 magnitudes of extinction ( $A_V = 1.19$  at  $6563\text{\AA}$ ) independent of  $L_{H\alpha}$ . At these epochs, quenched massive galaxies are increasingly rare, so the comparison should be more meaningful than at  $z = 0$ .

At both epochs, the no-winds run overproduces the number of galaxies with  $\text{SFR} \lesssim 100 M_\odot/\text{yr}$ , sw overproduces galaxies with  $\text{SFR} \gtrsim 1 M_\odot/\text{yr}$ , and cw underproduces galaxies with  $1 \lesssim \text{SFR} \lesssim 100 M_\odot/\text{yr}$ . The momentum-driven scalings model fares reasonably well at both redshifts. At  $z \sim 1$  it still slightly overproduces high-SFR galaxies, which is the onset of a trend that becomes much more prominent by  $z = 0$ . At  $z \sim 2$  the bright end matches well, while the faint end is modestly steeper than observed. Note however that Hayes, Schaerer, & Östlin (2010) derive a steeper  $H\alpha$  luminosity function from their faint-end data alone ( $\alpha = 1.72$  instead of  $\alpha = 1.60$  for the fit shown here). Furthermore, convolving in the uncertainties in  $M_*$  determinations will tend to make the predicted  $\Phi_{\text{SFR}}$  shallower, as we showed with the GSMF in Figure 1. Hence the discrepancies may not be significant.

Overall, the simulated star formation rate functions of the constant- $\eta$  models display a three-tiered trend arising from differential wind recycling as seen in the GSMF. The form and evolution of  $\Phi_{\text{SFR}}$  provides independent constraints on how outflows govern star formation across cosmic time. At low- $z$ , all current models produce too many rapidly star-forming galaxies, owing to a lack of quenching feedback in massive galaxies. At  $z \gtrsim 1$ , the momentum-driven scalings simulation predicts  $\Phi_{\text{SFR}}$  in good agreement with available  $H\alpha$  data, while other wind models do not.

## 4 SPECIFIC STAR FORMATION RATE

The specific star formation rate (sSFR) measures the intensity of ongoing versus past-averaged star formation, so it provides an important barometer for how a given galaxy has assembled. It also most directly governs the observed colors of galaxies. The main sequence of galaxies reflects a relation between sSFR and  $M_*$ , and yields important insights into galaxy growth. In this section we study the specific star formation rate in our simulations. We will particularly focus on how the slowly-evolving equilibrium between inflows, star formation, and outflows governs the behavior of sSFR as a function of mass and epoch.

### 4.1 Specific Star Formation Rate vs. $M_*$

Figure 3 shows the sSFR of galaxies at  $z = 0$  in our four wind models. A running median within mass bins is shown in magenta with  $1\sigma$  variance; this does not include the non-starforming galaxies shown along the bottom of the plot, which do not substantially change the median except at the lowest masses in the constant- $\eta$  models (we will return to this in §5). The points are color-coded by gas fraction within

each mass bin, blue meaning high  $f_{\text{gas}}$  ( $> 0.5\sigma$  above median), red for low, and green in between. Here we define gas fraction as  $f_{\text{gas}} \equiv M_{\text{gas}}/(M_{\text{gas}} + M_*)$ , with  $M_{\text{gas}}$  including all gaseous phases in the star-forming ISM. Observations of galaxies are shown as the thick lines from a compilation of GALEX and SDSS data by Salim et al. (2007): Solid line represents the median sSFR for all galaxies classified as having no AGN content in a Baldwin, Phillips, & Terlevich (1981) diagram, while the dashed double power-law represents those classified as red ( $\text{NUV}-r > 4$ ). The observed median for all galaxies drops sharply above  $\gtrsim 10^{11} M_\odot$  as red and dead galaxies dominate in that mass range.

Simulations generically produce a fairly tight relation between SFR and  $M_*$  (e.g. Davé et al. 2000; Finlator et al. 2006). In all cases, the relatively flat  $\text{sSFR}(M_*)$  implies that star formation rate scales roughly linearly with stellar mass, and at the high-mass end in all cases the scaling is sub-linear. The basic similarity indicates that the sSFR is not highly sensitive to feedback, as has been noted previously (Davé 2008; Dutton et al. 2010). The basic reason is that, to first order, feedback processes reduce SFR and  $M_*$  in conjunction, thereby keeping sSFR roughly similar. All models produce massive galaxies that are forming stars vigorously, in contrast with observations that indicate most galaxies at high masses are passive, indicating the need for some quenching mechanism (Gabor et al. 2011). All models also produce a population of low-mass galaxies that are not forming stars; these are predominantly satellite galaxies, and will be discussed in §5.

The basic trends in this plot can be understood in the context of a balance between accretion, outflow, and star formation. As shown in Finlator & Davé (2008), galaxies live in a slowly-evolving quasi-equilibrium between these quantities, such that

$$\dot{M}_{\text{inflow}} = \dot{M}_{\text{outflow}} + \text{SFR}, \quad (4)$$

where the first two terms are the mass inflow and outflow rates, respectively. We can rewrite this using the definition of the mass loading factor  $\eta \equiv \dot{M}_{\text{outflow}}/\text{SFR}$ , so that

$$\text{SFR} = \dot{M}_{\text{inflow}}/(1 + \eta). \quad (5)$$

This equation, while simple, implicitly makes some non-trivial assumptions. First, it assumes that the variations in the inflow rate are slow compared to the rate of processing gas into stars, so that galaxies are never strongly out of equilibrium (e.g. this is not valid during major merger events). Second, it assumes that galaxies do not collect large reservoirs of gas and then process it, but rather process gas as it is made available to the ISM (from inflows and outflows); we call this “supply-regulated” star formation, to distinguish it from other scenarios where gas aggregates in or around galaxies before being consumed rapidly (e.g. Eggen, Lynden-Bell, & Sandage 1962; Maraston et al. 2010). Third, there is no explicit dependence on cosmic epoch or environment, as these are assumed to be of secondary importance in galaxy growth. Fourth, it neglects additional reservoirs of gas such as stellar mass loss (Schaye et al. 2010; Leitner & Kravtsov 2010) and wind recycling (Oppenheimer et al. 2010) that are particularly important at late times, and hence this equation is expected to be more valid at earlier epochs. We will show in this paper and Paper II (see also Finlator & Davé 2008) that

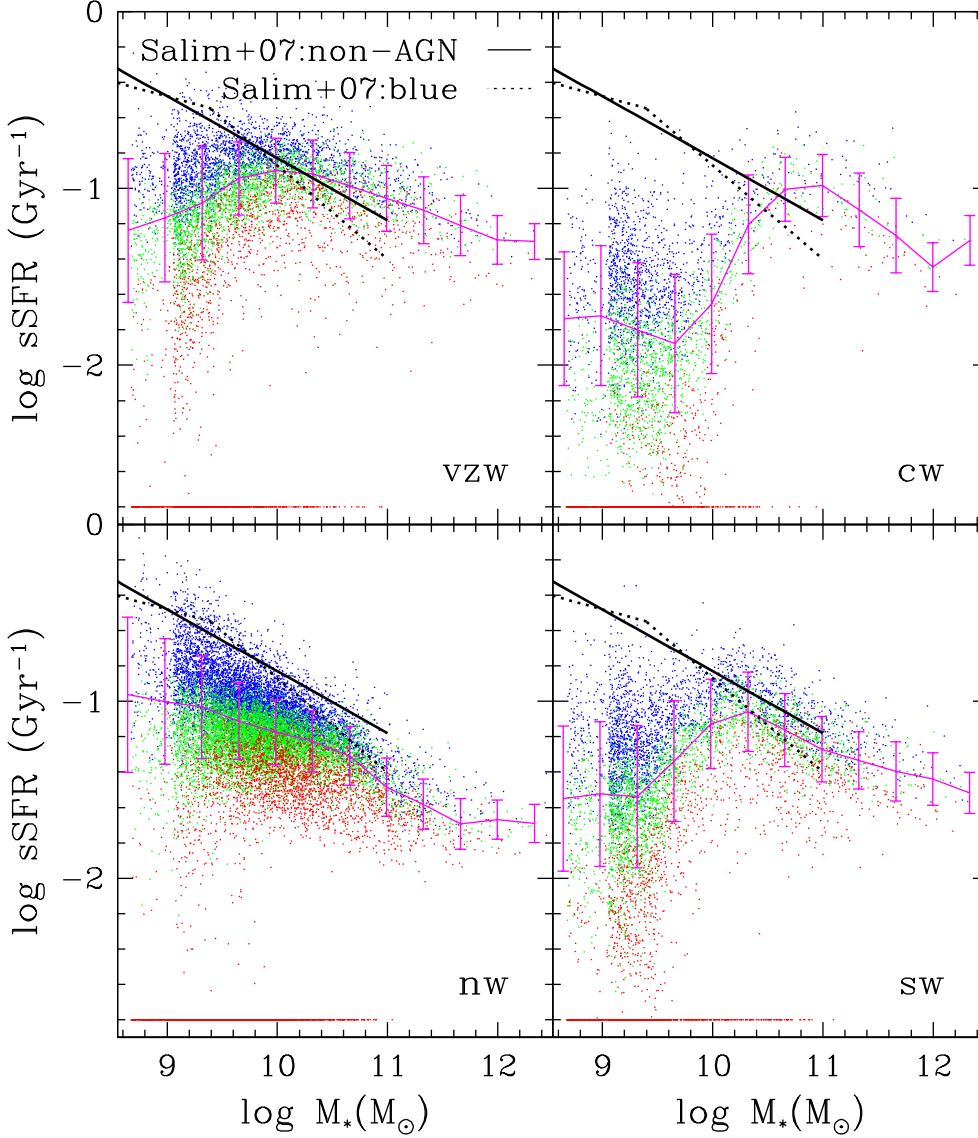


**Figure 3.** Specific star formation rate ( $\text{sSFR} \equiv \text{SFR}/M_*$ ) as a function of stellar mass at  $z = 0$  in our r48n384 series of simulations employing our four galactic outflow scalings: momentum-conserved winds (upper left), constant winds (upper right), no winds (lower left), and slow winds (lower right). Points are color-coded by gas fraction within each stellar mass bin: Galaxies with  $f_{\text{gas}}$  exceeding  $0.5\sigma$  above the median are blue, less than  $0.5\sigma$  below the median are red, and in between are green. Galaxies with  $\text{sSFR} = 0$  are shown as red points along the bottom. A running median is shown in magenta, excluding non-starforming galaxies. Thick lines show observed GALEX+SDSS best-fit relations (Salim et al. 2007) for non-AGN star-forming galaxies (solid) and blue galaxies with  $NUV - r < 4$  (dashed, broken power law).

simulated galaxy properties generally follow those expected from the equilibrium relation (eq. 4), although more so at early epochs, suggesting that at least in these models, the above assumptions are broadly valid.

Within the context of this equilibrium model, let us return to examining sSFRs. In the no-wind case,  $\eta = 0$ , so the trend of  $\text{sSFR}(M_*)$  reflects the inflow rate into galaxies of a given  $M_*$ . Owing to the growth of hot gaseous halos that retard inflow in larger halos (e.g. Kereš et al. 2005; Dekel & Birnboim 2006), the sSFR is smaller at larger masses. This is one manifestation of downsizing, namely star formation rate downsizing as defined in Fontanot et al. (2009). This model also produces archaeological downsizing, which means that larger galaxies have older stellage popu-

lations (also called “natural downsizing” Davé et al. 2006; Neistein, van den Bosch, & Dekel 2006), as we will show in §5.3. Note that these downsizing trends, while qualitatively in agreement with data, do not by themselves produce massive red and dead galaxies (Gabor et al. 2010). In the no-wind case, the slope of  $\text{sSFR}(M_*)$  agrees well with observations, but the amplitude is too low by  $\sim \times 2$ . Hence paradoxically, while no winds produce far too much global star formation (and stellar mass), they produce too little star formation at a given stellar mass today. They also produce  $\sim \times 10$  more stellar mass for a given halo mass (Kereš et al. 2009a; Oppenheimer et al. 2010), so that the excess global star formation arises from too much star formation per halo, particularly at high and low masses.

The wind models deviate from the no wind case based on  $\eta(M_*)$  and wind recycling. In the cw and sw models, since  $\eta$  is constant, in the simplest scenario both SFR and  $M_*$  are reduced equally. This shifts a given galaxy down in  $M_*$  from the no-wind case by a factor of  $(1 + \eta) = 3$ , when the mass is small enough that winds don't recycle (i.e. the effective mass loading factor is identical to the input mass loading factor). Since the overall slope of the no-wind case is negative, this results in a lower sSFR at a given mass. An additional suppression is provided by preventive feedback from heat added to surrounding gas by winds (van de Voort et al. 2010), which lowers the accretion rate and hence sSFR at a given  $M_*$ . This is particularly noticeable in the cw case which adds substantial energy to surrounding gas and the even the IGM (Oppenheimer & Davé 2006). At the highest masses, all winds are gravitationally and hydrodynamically trapped, resulting in an effective mass loading factor of  $\eta \approx 0$  as discussed in §2.2, and so also follows the no-wind case trend with a slightly higher amplitude. The reason for the amplitude difference is that wind recycling removes mass from small systems and adds it back into larger systems at later epochs. Hence wind recycling shifts star formation from low to high masses, an effect that is stronger with the higher wind speeds owing to the increase in the recycling time and increasing preventive feedback from added heat. Both these models are in poor agreement with observations, as they have too low sSFR by up to an order of magnitude at the low-mass end, and the observations do not indicate any positive-slope feature in the predicted mass range.

In the case of momentum-conserved winds,  $\eta$  varies with mass. At the lowest masses where there is no wind recycling,  $\eta \propto \sigma^{-1} \propto M_{\text{gal}}^{-1/3} \propto M_*^{-1/3}$  (roughly, although in detail smaller galaxies tend to have lower stellar fractions, making the slope slightly shallower), since our wind model ties  $\sigma$  directly to the galaxy baryonic mass  $M_{\text{gal}}$  as identified by our group finder (see eq. 6 of Oppenheimer & Davé 2008). Hence the sSFR shows a slope that exceeds the no-wind case by roughly  $1/3$ . This by itself would result in a slope of around zero. But differential wind recycling produces an additional effect, which in this model is more gradual and occurs over a wider range in mass than in the constant- $\eta$  cases. At intermediate masses, the additional fuel from recycling causes a positive slope for  $\text{sSFR}(M_*)$ , for the same reason as in the constant- $\eta$  case except the effect is more gradual. Firmani, Avila-Reese, & Rodriguez-Puebla (2010) also pointed out that wind recycling tends to increase the slope of  $\text{sSFR}(M_*)$ . At the largest masses, the slope again reverts to the no-wind case as recycling times are very short (Oppenheimer et al. 2010), so winds have little effect.

The gradual rolling of the slope of  $\text{sSFR}(M_*)$  is also seen in observations, but it less pronounced and really only evident at masses below what are plotted here (see Figure 16 of Salim et al. 2007). Even at  $M_* \lesssim 10^9 M_\odot$ , the observed  $\text{sSFR}(M_*)$  has a negative slope (Salim et al. 2007), whereas this model predicts a positive slope. We will see in Paper II that this is also reflected in the relation between gas fraction and  $M_*$ , which has a turnover to low masses that is likewise absent in observations. This could signify that wind recycling should be more effective in small systems, or perhaps less material should be ejected from these systems in the first place. Just as with the faint end of the high-redshift GSMF, this highlights that even our most successful model has dif-

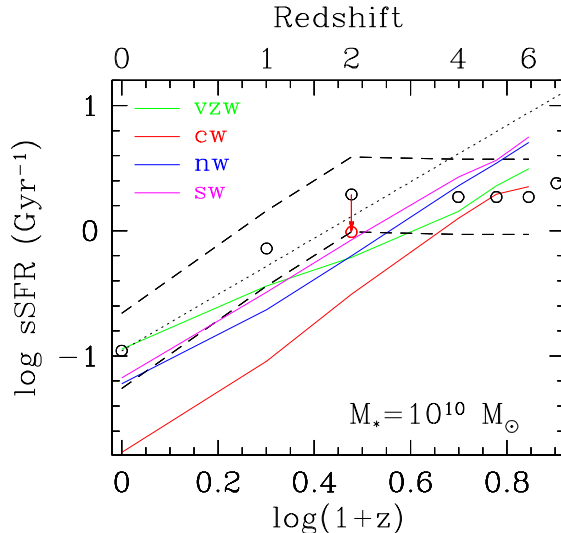


**Figure 4.** Evolution of the specific star formation rate at a stellar mass of  $M_* = 10^{10} M_\odot$  from  $z = 6 \rightarrow 0$  in our r48n384 series of simulations employing our four galactic outflow scalings. Observations are shown at  $z = 0, 1$  from Elbaz et al. (2007) and at  $z \geq 2$  from González et al. (2010). The downward arrow on the data point at  $z \sim 2$  indicates the  $\sim \times 2$  lowering of the UV-derived SFR based on *Herschel* data. Dashed lines show the typical observed  $1\sigma$  variance about the  $M_*$ –SFR relation (Noeske et al. 2007; Daddi et al. 2007). The black dotted line shows a power-law scaling of  $(1+z)^{2.25}$  as predicted from cold accretion-driven galaxy growth.

ficulty correctly reproducing observations of dwarf galaxies. We will return to this point in §5.3.

An interesting second-parameter trend is indicated by the color of the simulated data points. Galaxies with high gas fractions at a given  $M_*$  lie above the mean sSFR relation, and those with low gas fractions lie below. This is not surprising since the presence of gas drives star formation based on our assumed star formation law, but it provides an interesting generic prediction (independent of outflows) of this class of models where star formation is driven by accretion. Such a trend would not be expected, for example, if mergers drove elevated SFRs at a given  $M_*$ ; in that case, it is the gas configuration rather than overall gas content that drives elevated SFRs, as gas is much more concentrated in mergers owing to tidal dissipation (e.g. Mihos & Hernquist 1996). In Paper II we will discuss second-parameter dependences of the relationships between stellar mass, metallicity, and star formation rate in much greater depth, all within the context of the aforementioned equilibrium model (eq. 4) for galaxy growth.

## 4.2 Specific Star Formation Rate Evolution

Figure 4 shows the evolution from  $z = 6 \rightarrow 0$  of the specific star formation rate at a particular stellar mass of  $M_* = 10^{10} M_\odot$  in our four wind models. This mass is chosen because observations can directly measure sSFR at this mass at all epochs (with small extrapolations), and it is well-resolved by simulations but is expected to be negligibly affected by quenching feedback. In the simulations, this

sSFR is computed as the median sSFR within a stellar mass bin of  $\pm 0.25$  dex around  $10^{10} M_{\odot}$ .

Most models show a characteristic evolution of the sSFR which is essentially a power law in  $(1+z)$ . The fundamental physics giving rise to this is gas inflow driven by growth of structure. In the cold accretion paradigm that captures the basic behavior in hydrodynamic simulations (e.g. Kereš et al. 2005), the amount of gas inflowing into the star forming region is correlated with the gas inflowing at the halo virial radius, since cold streams efficiently channel material to the center of the halo (Dekel et al. 2009). Feedback processes that strongly impact the surrounding gas to retard infall can cause significant deviations from this (van de Voort et al. 2010), but let us set that aside for now to examine the implications of this simplest scenario. The amount of gas entering the virial radius can be estimated by the total mass accretion rate times the baryon fraction. The total mass accretion rate onto halos has been well measured in simulations (Dekel et al. 2009), and scales with redshift as  $(1+z)^{2.25}$ .

The scaling of  $(1+z)^{2.25}$  is indicated by the dotted line, arbitrarily normalised to the observed  $z=0$  sSFR. The no-wind and slow-wind cases follow this power law essentially at all redshifts. The no-wind case is easy to understand, since there is no additional physics regulating star formation beyond accretion. The slow-wind case also follows this because it simply ejects a constant two-thirds of the accreted material. Hence the SFR reduction translates into a similar reduction in  $M_*$ , so the sSFR evolution is nearly identical to the no-wind case. In the sw case, two additional processes are at work: Feedback heats surrounding gas to retard accretion into the ISM, which is countered by additional accretion provided by recycled winds. Note that at this stellar mass, about half the  $z=0$  accretion is recycled winds (Oppenheimer et al. 2010), and both recycling and heating increase to low redshifts. The impact of these processes does not appear to be large (barring a remarkable cancellation), as the net effect is only a slight increase in sSFR in the sw model over the no-wind case.

The constant wind case shows a substantial departure from no-winds, with sSFR lower by  $\sim \times 2 - 5$ , increasing at late times. As discussed previously, this model produces significant heating of surrounding gas, substantially retarding inflow into the ISM from the virial radius (Oppenheimer et al. 2010; van de Voort et al. 2010). This effect becomes stronger at low- $z$  as feedback energy accumulates in the IGM, as evidenced e.g. by a much higher fraction of cosmic gas in the Warm-Hot Intergalactic Medium in this model (Davé et al. 2010a). At  $M_* = 10^{10} M_{\odot}$ , recycling is rare in this wind model (Oppenheimer et al. 2010), so the net effect is to strongly lower the sSFR relative to the no winds case.

In contrast, the momentum-driven wind scalings model increases the sSFR relative to no winds. In this case, the relationship to no-winds is not so straightforward to understand, because the mass loading factor depends on galaxy mass and epoch. Overall, the amount of energy input in vzw is smaller than in cw. Recycling is dominant at late times at  $M_* \sim 10^{10} M_{\odot}$ , but at early epochs it is not infrequent. The net effect is larger suppressions of the sSFR at early epochs, while at late times the wind recycling at this mass causes the sSFR to be higher relative to a simple inflow model extrap-

olated from high- $z$ . Hence the vzw model yields a shallower evolution of sSFR( $z$ ) because it suppresses star formation at early epochs and later recycles that material into galaxies.

Observations show a very rapid rise from  $z=0 \rightarrow 2$ , and then essentially no evolution out to very high redshifts (Daddi et al. 2007; Stark et al. 2010; González et al. 2010). Bouché et al. (2010) showed that this is difficult to reproduce in a simple accretion-driven scenario, and they argued for a rather radical modification to the galaxy formation paradigm in which no stars formed in halos with virial masses less than  $10^{11} M_{\odot}$  (as well as above  $10^{12} M_{\odot}$ ). This strongly suppresses early star formation until the characteristic mass of star-forming halos exceeds this threshold mass, at which point it reverts to the accretion-driven scaling. Clearly this hypothesis is incorrect today; there is no evident feature in the galaxy population around halo masses of  $\sim 10^{11} M_{\odot}$ , unlike at  $\sim 10^{12} M_{\odot}$  where many transitions occur. It is also difficult to accommodate at high- $z$ , as smaller halos need to form stars to reionise the Universe and form observed high- $z$  galaxy populations (Muñoz & Loeb 2011). Nevertheless, while implausible, this scenario correctly emphasizes that some process must suppress high-redshift star formation significantly in order to match current sSFR evolution observations.

The observations are themselves uncertain to some extent, particularly at high redshifts. For instance, the original  $z \sim 2$  data point (black circle) was taken from dust-corrected UV-derived star formation rates of star-forming BzK galaxies (Daddi et al. 2007). Recent *Herschel* data characterizing the infrared continuum of such sources suggests that the extinction corrections were overestimated by up to  $\sim \times 2$  (Nordon et al. 2010); this modification is shown by the red arrow and circle in Figure 4. Prior to this correction, the data exceeded the accretion rate evolution, making it difficult to reconcile this evolution within the cold accretion paradigm. This prompted Davé (2008) to make the radical suggestion that the IMF may evolve with redshift, so that the true SFR's were lower by  $\sim \times 3$ . If the *Herschel*-derived correction is right, the  $z \sim 2$  data point is now consistent with being powered by ongoing accretion, making it viable within the cold accretion paradigm. Davé (2010a) pointed out that there still may be a problem with respect to the momentum-driven scalings model; this may be particularly true if the corrections at these masses (which are not directly constrained by *Herschel* data) are less than a factor of two (see also Nordon et al. 2010). But this is no longer a fundamental difficulty, and this level of discrepancy could in principle be alleviated by modifications of the feedback prescription. Indeed, Genel et al. (2011) find that doing high-resolution disk simulations using a momentum-conserved feedback model with somewhat different parameters results in galaxies that are in very good agreement with (corrected) sSFR data at  $z \approx 2$ .

The slope  $\beta$  of the main sequence (defined by  $\text{SFR} \propto M_*^{\beta}$ ) is also observed to evolve downwards from being unity at high- $z$  (Stark et al. 2010; Labbé et al. 2006), to  $\beta \approx 0.9$  at  $z \sim 1-2$  (Daddi et al. 2007; Elbaz et al. 2007), to  $\beta \approx 0.7$  at  $z \lesssim 1$  (Noeske et al. 2007) down to  $z \sim 0$  (Brinchmann et al. 2004). There is some sensitivity to selection effects, particularly in how one chooses a sample of star-forming galaxies at the massive end; the preponderance of low-sSFR massive galaxies particularly at low- $z$  pulls the slope down de-



pending on how many such systems are included in the fit. Hence it is not straightforward to compare to our models where we do not reproduce large passive galaxies. In general, our momentum-conserved winds case produces slopes of  $\beta \approx 0.9 - 1$ , roughly independently of redshift, and the no-wind case produces a shallower slope. For the constant- $\eta$  models  $\beta$  is ill-defined as they show a strong three-tiered behavior. The trend of the slope becoming more shallow with time is therefore not obviously evident even in our favored model. While this may be a consequence of the lack of quenching feedback in massive galaxies, we note that the semi-analytic model of Somerville et al. (2008) includes AGN feedback but still produces a slope around unity for the present-day main sequence.

In summary, the evolution of the specific star formation rate encodes information about the feedback processes that have regulated star formation up to that epoch. Hence this is a critical quantity to measure with upcoming surveys. The fundamental driver is the gas accretion rate onto halos, which evolves as  $(1+z)^{2.25}$ , but feedback can modify this by either retarding accretion onto the galaxy or adding recycled wind accretion. Matching observations that suggest a significant departure from this scaling at  $z \gtrsim 2$  requires suppressing star formation at early epochs. Of the feedback models examined here, only the momentum-conserved scalings case works in this sense, though it is still well away from the unevolving sSFR seen from  $z \sim 4 - 7$ . Observations at these epochs remain fairly uncertain (see e.g. Schaerer & de Barros 2010), so we await more robust constraints from upcoming surveys.

## 5 SATELLITE VS. CENTRAL GALAXIES

The equilibrium paradigm for galaxy evolution introduced earlier is appropriate for central galaxies, because cold accretion channels material to the centers of halos. Satellite galaxies, in contrast, must scavenge their fuel from ambient halo gas, and therefore can be impacted by a range of processes related to their surrounding environment. Satellite galaxies could thus display a broadly different class of properties than central galaxies, for which environment is not a major driver except through wind recycling. Here we investigate the properties of satellite vs. central galaxies in our simulations, contrasting the statistics we have examined earlier between the satellite and central galaxy populations. We particularly focus on dwarf galaxies where many environmental processes could play a large role.

### 5.1 Satellite Fraction

Figure 5 shows stellar mass functions as in Figure 1 (black curves), subdivided into central galaxies (magenta curves) and satellite galaxies (cyan curves). Solid curves show  $z = 0$  results, while dashed curves show  $z = 2$ . Smaller panel below each main panel show the fraction of satellite galaxies as a function of stellar mass, also at  $z = 0$  (solid) and  $z = 2$  (dashed). Only the r48n384 series of runs are shown in this plot.

Satellite galaxy mass functions are, for the most part, simply scaled-down versions of the central galaxy mass functions. They display the same features arising from differen-

tial wind recycling. In general, the properties of satellites appear to be established when they are central galaxies in their own halo, and are not dramatically affected by falling into a larger halo. This is broadly consistent with trends inferred from halo occupation distribution models of galaxy clustering within dark matter halos (e.g. Conroy et al. 2006).

For all models at  $z = 0$ , central galaxies dominate by number at all resolved masses. This may be surprising, as it is often assumed that most small galaxies are satellites, and that the fraction of satellites increases strongly to small masses. The no-wind model does show an increase in satellite fraction to lower masses, but only mildly so. In contrast, the wind models show a satellite fraction that is approximately constant at one-third of all galaxies for  $M_* \lesssim M^*$ . For  $M_* > M^*$  the satellite fraction decreases, although it is high again at very large masses – these are satellites in galaxy groups where the halo occupation distribution is steeply rising (e.g. Berlind et al. 2003). These results agree with those obtained by van den Bosch et al. (2008, see their Figure 8) based on the conditional luminosity function constrained by the 2dF Galaxy Redshift Survey, and recent SAMs also yield similar trends (Guo & White 2010). At  $z = 2$ , there are even fewer satellite galaxies at a given stellar mass, typically only around 20% of all galaxies for  $M_* \lesssim 10^{11} M_\odot$ . Hence dwarf galaxies are not typically satellites, but rather central galaxies in small halos.

The relatively constant (and low) satellite fraction has a significant implication for galaxy formation. It means that that whatever physics is responsible for establishing the mass function and other such ensemble-averaged observables must predominantly govern central galaxies, not satellites (see also Fontanot et al. 2009). It is not possible, for instance, to alter satellite galaxy physics to reconcile the steep faint-end GSMF slope in the constant- $\eta$  or no-wind simulations with observations. This is even more true at higher redshifts. Hence the evolution of the ensemble population of galaxies is governed by central galaxies, and understanding galaxy evolution is, to first order, tantamount to understanding how central galaxies form and grow.

### 5.2 Quenched Satellites

Figure 6 shows birthrates for galaxies in our four wind models, separated into central (blue) and satellite (red) galaxies. The birthrate is defined as the specific star formation rate multiplied by the time over which the galaxy has been forming stars; the sSFR values are noted on the right axis, for comparison with Figure 3. Davé (2008) showed that the timescale for star formation in most galaxies is reasonably well approximated by the Hubble time less 1 Gyr, since none but the largest galaxies (today) form stars in the first Gyr. A running median birthrate and lines enclosing 25% and 75% of galaxies in a given mass bin are given by the solid and dashed lines, for centrals (magenta) and satellites (cyan).

Birthrates are typically around unity for all models. At the massive end all models show a negative slope in birthrates with  $M_*$ , indicative of archaeological downsizing. At small masses, this can invert owing to differential wind recycling as discussed in the previous section. Overall, however, star-forming galaxies show generically smooth and fairly constant SFHs over much of cosmic time to

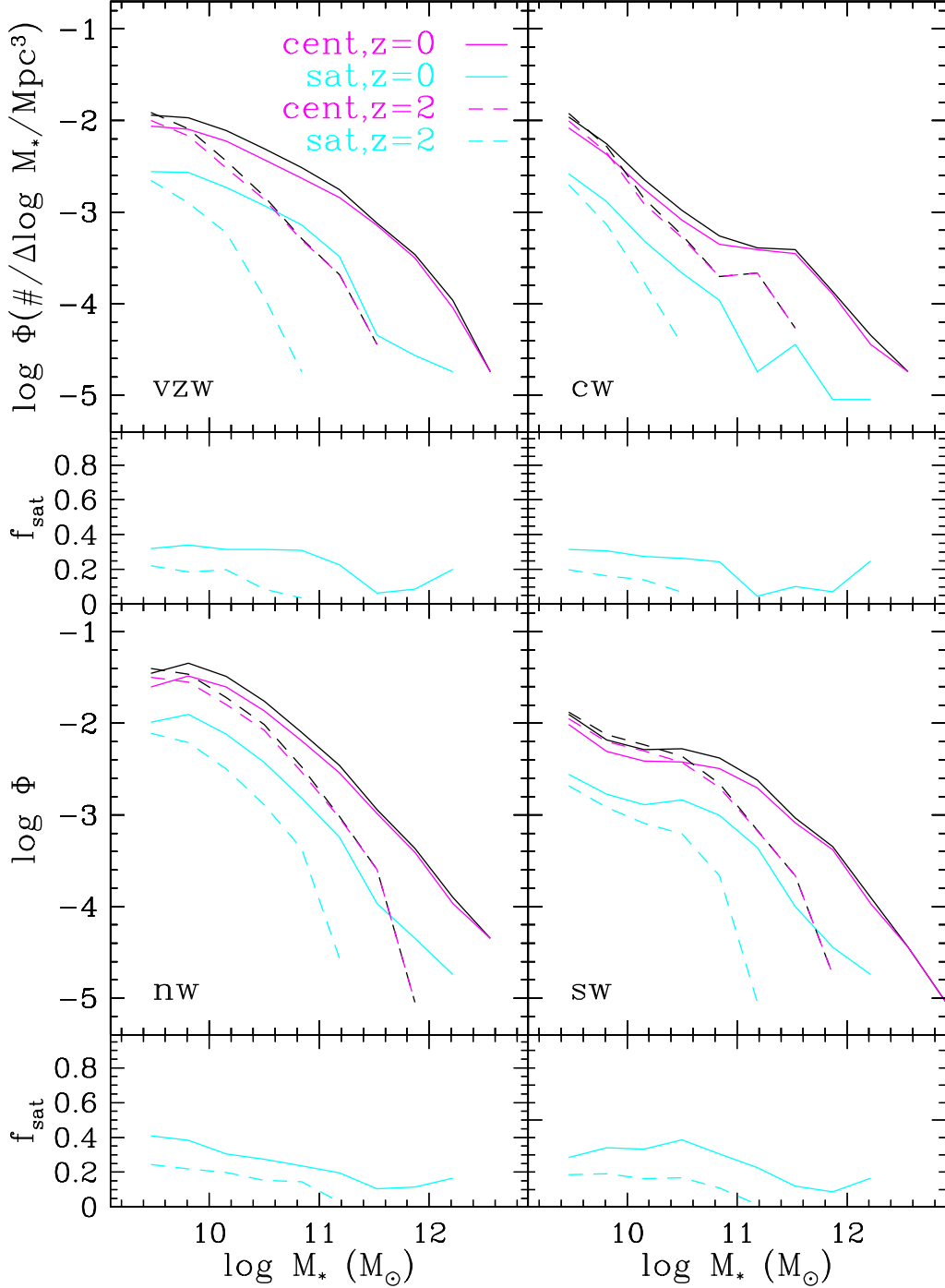


**Figure 5.** Four larger panels show stellar mass functions at  $z = 0$  (solid lines) and  $z = 2$  (dashed lines) for our four r48n384 simulations. Black lines are the total mass functions (reproduced from Figure 1), which are subdivided into centrals (magenta) versus satellites (cyan). Accompanying smaller panels below each large panel show the fraction of satellite galaxies as a function of  $M_*$  at  $z = 0$  (solid) and  $z = 2$  (dashed).

$z \sim 0$  (Davé 2008), similar to that inferred for the Milky Way.

There are a significant number of galaxies with no ongoing star formation (i.e. “quenched”), predominantly at low masses. The smaller panels show the fraction of quenched central (magenta) and satellite (cyan) galaxies as a function of  $M_*$ . There are a few small central galaxies with zero instantaneous SFR’s. It is not clear what these are; one pos-

sibility is that they are actually quenched satellites whose orbits carry them outside the virial radius calculated by our spherical overdensity halo finder, and therefore are identified as centrals. Another possibility is that quenching is partly numerical, since this may impact a satellite galaxy’s ability to cool gas from a hot halo. Since they are very few in number, we will leave a detailed investigation of these possibilities for the future.



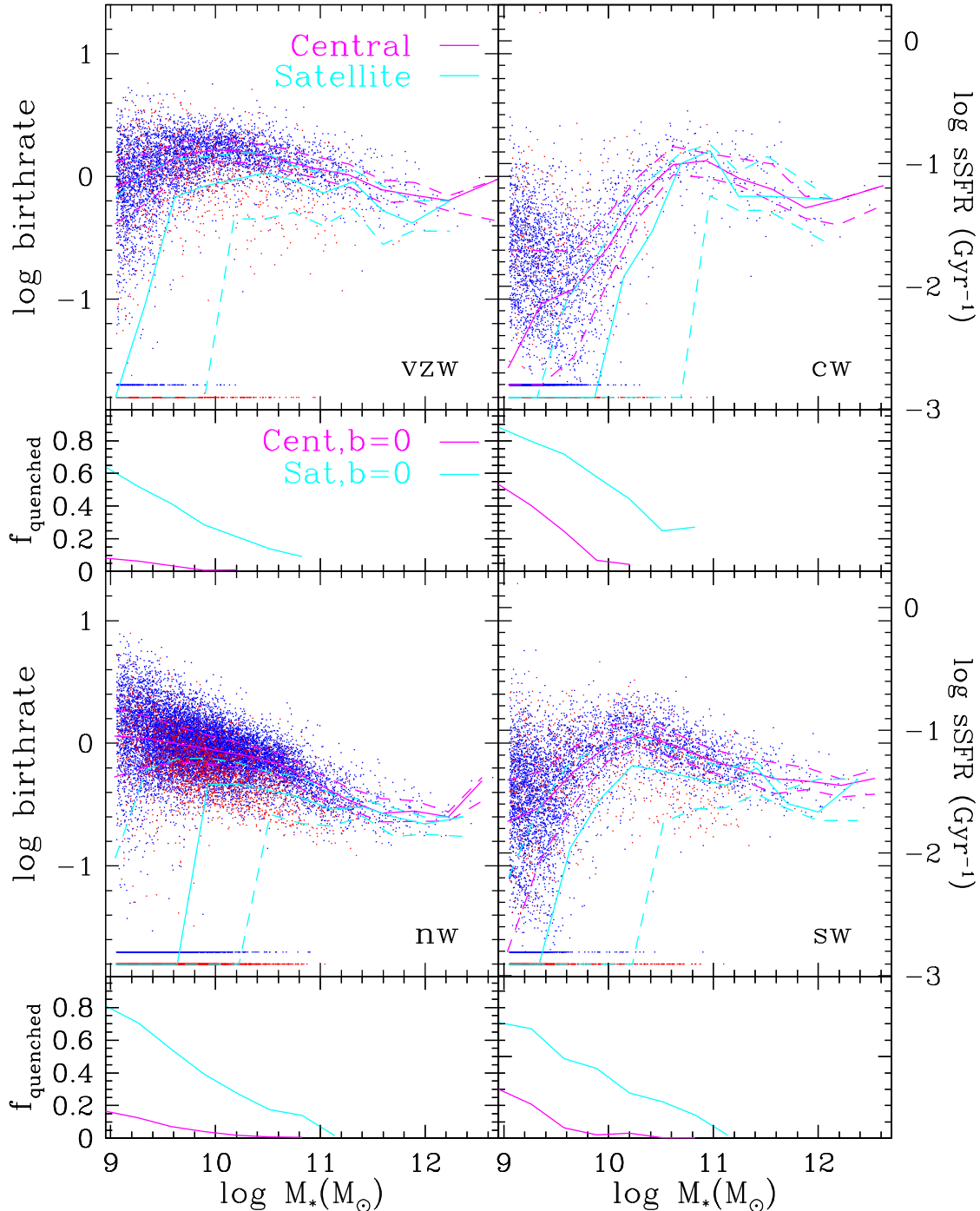


**Figure 6.** Larger panels show the birthrate (i.e.  $t_{\text{SFR}}\text{SFR}/M_*$ , where  $t_{\text{SFR}} = t_{\text{Hubble}} - 1\text{Gyr}$ ) for galaxies from our r48n384 runs at  $z = 0$  color-coded by central (blue) and satellite (red) in our four wind models. Galaxies with  $\text{SFR} = 0$  (“quenched”) are shown along the bottom of the plot. Running median (solid curves), including quenched galaxies, are shown for central galaxies (magenta) and satellites (cyan). Dashed above and below show running 75% and 25% percentiles, respectively. Small panels below show the fraction of quenched galaxies (having birthrate  $b = 0$ ) in a given mass bin for centrals (magenta) and satellites (cyan).

The satellite quenched fractions become large towards small masses. Below a few  $\times 10^9 M_\odot$ , the median sSFR drops to zero for satellites in all models. Even above this mass, satellites show lower typical sSFR’s than central galaxies, hence environmental processes can affect even large satellite galaxies. The different wind models (including no winds) show only minor differences in terms of quenched satellite

fraction, despite significant differences in sSFR. This indicates that it is not outflows that are responsible for quenching satellites, and instead is some process(es) related to environment that depends more on the growth of structure common to all models.

Possible environmental processes that quench satellites are ram pressure stripping, tidal harassment, and strangu-

lation (i.e. cutting off of the gas supply). Simha et al. (2009) showed that, in SPH simulations similar to ours, quenching of a galaxy occurs on a  $\sim 1$  Gyr timescale after entering another galaxy’s halo. The process is gradual because sub-halos retain their identity for quite some time after entering a larger halo, so the satellite does not immediately see the full effect of the hot gas in the larger halo. In the cold accretion paradigm, the gas cooling along filaments tends to fall to the center of the halo, and hence galaxies that turn into satellites become disconnected from their feeding filaments. But strangulation cannot be the entire story, because the gas consumption timescales for these systems are of order a few Gyr (as we will show in Paper II), whereas quenching occurs on a timescale of  $\lesssim 1$  Gyr. Hence harassment and stripping must be playing a role. Unfortunately, while the exact processes that drive satellite quenching are interesting, they are a great numerical challenge to model properly (e.g. Agertz et al. 2007), and the numerical resolution and methodology used here is probably insufficient to make robust quantitative statements.

Although there are seen to be a significant number of dwarf galaxies with little or no ongoing star formation, SDSS data (Weinmann et al. 2006; van den Bosch et al. 2008) actually indicate a trend opposite to that predicted here, namely a smaller fraction of red satellites (and centrals) at smaller masses. One difference may be that these analyses defined red based on a color cut between the red sequence and blue cloud, which does not straightforwardly correspond to being fully quenched or not; the observed galaxies may simply have lower specific SFRs. Interestingly, a recent semi-analytic model that is more successful than our simulations at matching a wider range of data still suffers from the same discrepancy, showing an upturn in red fraction at low masses (Kimm et al. 2009). Hence the qualitative discrepancy may hint at generic difficulties in modeling environmental effects in satellites within hierarchical models, and bears further investigation.

In summary, the fraction of satellite galaxies in our wind models is roughly constant with mass for  $M_* \lesssim M^*$  at around 20-30%, declining slightly with redshift. Their mass functions show trends similar to centrals, likely reflecting the fact that these trends are set when satellites were centrals. Satellites are increasingly quenched to smaller masses, reflecting environmental processes that gradually disconnect these galaxies from their feeding cold streams. High-mass quenching must arise from another source that is currently not included such as AGN feedback, but low-mass quenching can be understood as a result of environmental effects that are already included (at least in principle) in these types of models.

### 5.3 Stellar Ages and Dwarf Galaxy Evolution

We have seen that below masses of  $M_* \lesssim 10^{10} M_\odot$ , the wind models show a turn-down in sSFR and birthrate (and in Paper II we will see a similar turn-down in gas fraction), for both satellites and centrals. This is in contradiction with observations that show no such turn-down.

To investigate this further, we show in Figure 7 the mean (mass-weighted) stellar ages of galaxies as a function of  $M_*$ , for satellites (red) and centrals (blue), in our four wind models at  $z = 0$ . This is essentially an archaeologi-

cal downsizing plot, showing whether more massive galaxies have older stellar populations as generally observed. Running medians are shown for centrals (magenta) and satellites (cyan).

All models exhibit archaeological downsizing for galaxies at the massive end. But for the wind models, below some mass the trend reverses, and smaller galaxies begin to be progressively older. This is opposite to the trend observed by Pasquali et al. (2010) in a group catalog derived from SDSS (see their Figure 4). For the vzw and sw models, this happens at  $M_* \sim 10^{10} M_\odot$ ; above this mass, the ages are in reasonable agreement with data. They also show that satellites are slightly older than centrals at a given mass, which is also qualitatively as observed, although Pasquali et al. (2010) find the median mass-weighted age difference at  $M_* = 10^{10} M_\odot$  is  $\sim 0.1$  Gyr (becoming smaller to higher masses) while our wind models predict a smaller difference. The no-wind case shows an archaeological downsizing trend at all masses.

The mass where the turn-down happens is exactly the mass where the specific star formation rate turns over (Figure 6). We argued previously that this owes to wind recycling, in particular the lack of it in the smallest systems. Hence we begin to build a consistent story for the failure of wind models in the dwarf galaxy regime: The smallest galaxies in these models begin forming stars early, and owing to ejection of mass they lose their gas and cannot reacquire it as fast as larger galaxies. This is not because small galaxies are satellites: central galaxies show exactly the same trend, and most small galaxies are centrals anyway.

One possibility is that the simulations do not resolve the (supposedly) bursty star formation histories of dwarf galaxies, which could give rise to younger ages. It is true that our simulations lack the resolution to model internal resonances that can drive gas towards the center of galaxies during interactions, fueling a burst (Mihos & Hernquist 1996). However, recent data has strongly questioned whether bursts are common in dwarfs. Lee et al. (2009) used the volume-limited 11HUGS sample to show that the burst fraction, defined as having birthrate  $> 2.5$ , is only  $6^{+4}_{-2}\%$  in dwarfs (typically  $\lesssim 0.1 L^*$ ), comprising  $23^{+14}_{-9}\%$  of that population’s star formation. These numbers are similar to what is seen for more massive galaxies (e.g. Brinchmann et al. 2004).

In the small panels in Figure 7 we show the burst ( $b > 2.5$ ) fraction as a function of mass, for centrals (magenta) and satellites (cyan). It is generally quite low, and in our favored vzw model it is mostly independent of mass at  $\sim 5\%$  for  $M_* \lesssim 10^{10.5} M_\odot$ , in both satellites and centrals. In the no wind case, the burst fraction rises dramatically at small masses, but mostly in central galaxies not satellites. The three-tiered shapes of the birthrate curves in the cw and sw model result in odd behaviors in the burst fraction, and result in very low burst fractions for small systems. The favoured momentum-conserved wind case agrees well with observations of burst fractions, although the fraction of star formation in bursts is  $\sim 15\%$  which is  $\approx 1\sigma$  below that observed. This model’s concordance with data suggests that, contrary to popular wisdom, small dwarfs are not significantly burstier compared to larger star-forming systems.

The higher ages, steep high- $z$  GSMF, and lower sSFR’s for dwarfs suggest that wind models should suppress early star formation in smaller systems even more than is cur-

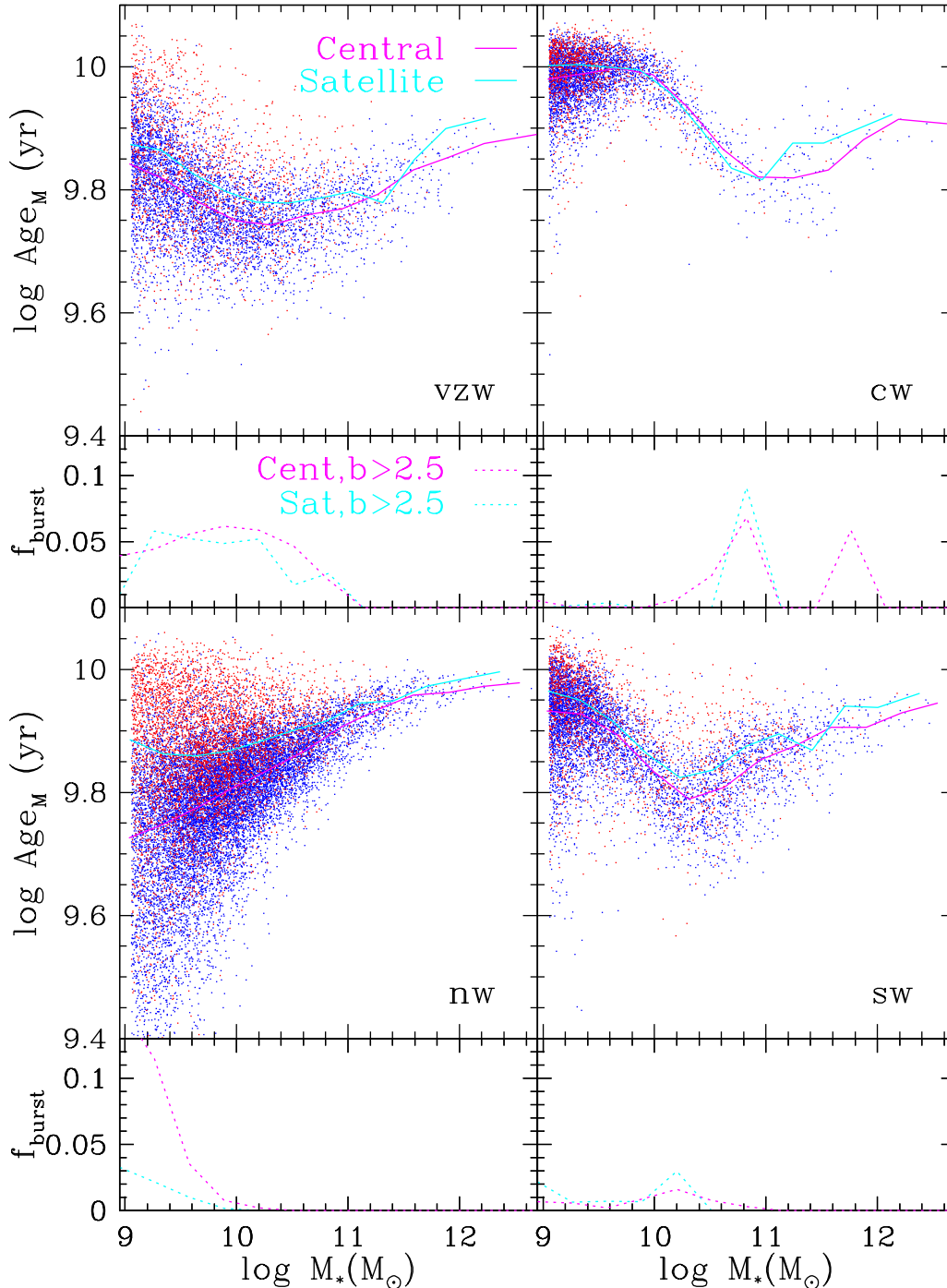


**Figure 7.** Larger panels show mean mass-weighted age of stars in galaxies in our r48n384 runs as a function of  $M_*$ , color-coded by central (blue) and satellite (red) in our four wind models at  $z = 0$ . Running median (solid curves), including quenched galaxies, are shown for central galaxies (magenta) and satellites (cyan). The smaller panels show the fraction of satellites identified as “bursting”, i.e. with birthrate  $b > 2.5$ , as a function of mass, for centrals (magenta) and satellites (cyan).

rently done in the momentum-conserved wind case, and produce a larger reservoir of gas for consumption at later epochs. This could arise if mass loading factors are larger at early epochs than assumed here, and/or wind speeds are reduced at late times such that these galaxies can reacquire their ejected gas. This could also arise if the star formation law is different in these systems owing to a less efficient conversion of atomic gas into molecular (e.g.

Robertson & Kravtsov 2008) – this would tend to delay star formation, providing a younger, more vigorously star-forming dwarf population today. Investigating this discrepancy further is likely to reveal new physical processes that are important for the evolution of small galaxies at all cosmic epochs.

## 6 SUMMARY AND DISCUSSION

Cosmological hydrodynamic simulations are now reaching a maturity level such that they can be informatively compared to observations of galaxies across cosmic time. This is a new era in this type of modeling, as past such efforts have generally produced quite poor agreement with data, and have been severely limited by dynamic range particularly when evolved to low redshifts. With improvement in both computing power and input physics, simulations can now plausibly reproduce a wider suite of observed relations (though still far from all), which in return can yield insights into the governing physics. A particularly important new physical aspect has been the incorporation of galactic outflows, originally motivated to explain IGM enrichment, and simultaneously having a wide-ranging impact on galaxies' stellar, gas, and metal content.

In this paper we present a study of how the stellar content and star formation rates of galaxies are impacted by galactic outflows. We concentrate on understanding the underlying physical drivers of these properties, and how observations can enlighten us on the way in which these drivers operate in the real Universe. To this end we present some comparisons with observations, showing that including outflows with momentum-conserved scalings provide the best overall match to the ensemble of observations considered in this work, although notable discrepancies remain. Given the broader success of this class of models in matching IGM (and other galaxy) properties, and that these scalings are consistent with those observed for outflows, this adds to the growing body of evidence that strong and ubiquitous outflows with these scalings are an important piece in understanding the overall evolution of galaxies.

The evolution of the stellar component can be broadly understood within the context of a cycle of gas inflow and outflow between galaxies and the IGM. This differs somewhat from the traditional view of galaxy formation in which halos and their mergers drive galaxy evolution. The cycle of baryons can at its most basic level be analytically represented by a slowly-evolving equilibrium between inflow, outflow, and star formation (eq. 4), where the outflows govern how much of the inflowing material turns into stars. The galaxy mass dependence of the outflow rate thus directly governs e.g. the GSMF, the specific star formation rate of galaxies, and galaxy ages. A particularly key aspect is the idea of differential wind recycling, in which material ejected returns to galaxies in a mass-dependent manner. This drives noticeable features in observable properties of galaxies as a function of mass, providing a way to constrain how outflows move material within the cosmic ecosystem surrounding galaxies. We reiterate that this scenario does not invoke the halo virial radius, environment, or mergers as playing a governing role in star-forming galaxy evolution. The cold streams feeding star-forming galaxies generally take no notice of the virial radius, are broadly unaffected by environment, and while such streams also carry in galaxies that merge, the mass growth rate in such mergers is sub-dominant (Dekel et al. 2009). In contrast, the virial radius, environment, and mergers seem to play a pivotal role in quenching star formation, and more generally in the evolution of massive halos hosting quiescent galaxies.

With that framework in mind, we summarize the key conclusions of this paper:

- Galactic outflows are required to suppress stellar mass growth at all epochs. The stellar mass function is quite steep and nearly a power law at high redshifts. At lower redshifts it develops a more pronounced three-tier behavior, where the middle tier reflects the steepness of differential (i.e. mass-dependent) wind recycling (Oppenheimer et al. 2010), and the higher and lower tiers tend towards the slope of the halo mass function. The middle tier (typically just below  $M^*$ ) becomes shallower with time owing primarily to wind recycling, which returns ejected material faster to more massive galaxies. Observations of the  $z \approx 0$  GSMF also show a three-tier behavior, and the momentum-conserved wind simulation comes closest to matching its behavior (although the three tiers are not obviously evident).

- The star formation rate functions show many of the same general features as the GSMF, but the detailed evolution, mass dependence, and dependence on outflows are somewhat different. Comparisons of these models to present-day data are hampered by their lack of quenching feedback in massive galaxies in our models. At  $z \gtrsim 1$  where massive quenched galaxies are less common, momentum-conserved winds produces a good match to the observed star formation rate function derived from H $\alpha$  data.

- The specific star formation rate's dependence on mass is governed by how the effective mass loading factor of outflows varies with stellar mass. The no-wind case shows too little star formation at a given  $M_*$ , despite having far too much star formation globally. The momentum-conserved wind model matches observations well at  $\sim 0.1 - 1 M^*$ , but all wind models show too little star formation at the smallest masses. This may indicate that there should be less mass loading or more wind recycling at the  $M_* \lesssim 0.1 M^*$  compared to what is currently in these models, or else the conversion of gas into stars is not being modeled properly in low-mass systems.

- The evolution of the sSFR is generally well-described as being driven by cosmic mass accretion into halos, which scales as  $(1+z)^{2.25}$ . The no-wind and slow-wind cases follow this trend at all redshifts. Observations do so at  $z \lesssim 2$ , but at  $z \gtrsim 2$  they depart from this scaling, indicating that small high-redshift galaxies must be significantly suppressed. The momentum-conserved wind model qualitatively yields this, but not enough to match current high- $z$  observations. Pinning down the sSFR evolution at  $z \gtrsim 2$  will have a major impact on understanding early galaxy evolution and feedback processes.

- Satellite galaxies are the minority of galaxies at all masses probed by these simulations (down to  $M_* \sim 10^9 M_\odot$ ), with a fraction of around one-third at  $z = 0$  independent of  $M_*$ . Hence understanding the growth of galaxies must focus on developing a model for central galaxies. The satellites' GSMF follows the same trends as that of centrals. However, there are many more non-star forming satellites than centrals, particularly at lower masses, owing to environmental effects wherein the satellites no longer effectively receive inflow from the IGM; this trend may be contrary to that observed. Small galaxies are at most only mildly more bursty than larger ones, and the burst fraction is small in accord

with observations. Our results challenge conventional notions that most small galaxies are bursty satellites.

Taking a broader view, it has long been recognised that the galaxy formation process must provide some feedback mechanism that preferentially suppresses mass growth at both high and low masses. In this paper we have advocated that it is galactic outflows that are primarily responsible for regulating the low-mass end. The advantages of invoking this particular mechanism are that (i) outflows are observed and seem to follow scalings that yield many desirable properties in models; (ii) they concurrently enrich the IGM at all cosmic epochs as observed; (iii) they lower the baryon content of halos preferentially to lower masses as observed (e.g. Davé 2010b); and (iv) they are an ejective feedback mechanism that works in conjunction with the cold accretion paradigm, in which it is difficult to prevent filaments from channeling gas efficiently into galaxies. There are other ideas to suppress low-mass star formation by regulating it as a function of mass internally within the ISM (i.e. by varying the star formation efficiency as a function of  $M_*$ ), or by preventing material entering the halo from accreting into small galaxies. But these scenarios must explain IGM enrichment separately, and must hide most of the gravitationally-accreted baryons in halos in some undetected form which is becoming increasingly difficult to accommodate (e.g. McGaugh et al. 2010; Dai et al. 2010).

While attractive, the idea of invoking outflows is not without its difficulties. For instance, the amount of mass being driven out of these galaxies is large, globally many times the amount of mass forming into stars. This is a generic result, because some process must suppress stellar masses by such large factors at the low mass end (Kereš et al. 2009a; Oppenheimer et al. 2010); in our models, this process is galactic outflows, as opposed to ISM physics or preventive feedback. The physical mechanism(s) that would drive such a sizeable amount of material out of galaxies is unclear. The canonical idea of driving outflows from overpressurized bubbles in the ISM tends to (when modeled) create holes by which energy and metals, but little mass, are ejected (e.g. Mac Low & Ferrara 1999), and there are difficulties with entraining cold clouds as observed without disrupting them. The scalings preferred by our current comparisons to data are those expected for radiation-driven winds, but it is not well known how far out the photons' momentum can drive dust, and how far out the dust remains coupled to the gas. For instance, Yoshida, Kawabata, & Ohiyama (2010) use spectropolarimetry to determine that the dust in M82 is moving outwards much more slowly than the gas, suggesting that the gas and dust are not strongly coupled. Furthermore, the momentum budget of typical stellar populations is, under the assumption of single photon scattering, insufficient to drive outflows as appear to be necessary, indicating that supernovae or other sources of energy are still required. Without a solid understanding of the dynamics driving outflows, simulations such as the ones presented here cannot be considered a complete description of the physics of galaxy formation. Fortunately, observations of outflows across cosmic time are gaining substantial traction (Martin 2005; Weiner et al. 2009; Steidel et al. 2010), providing empirical constraints for models while the theory of outflow propagation develops.

Our momentum-conserved winds provides the best match to data on star-forming galaxies of the four models considered here. But the agreement is only good in the rather narrow mass range from  $10^{10} \lesssim M_* \lesssim 10^{11} M_\odot$ . At larger masses, the current models require some additional quenching mechanism perhaps associated with AGN (e.g. Di Matteo et al. 2005; Croton et al. 2006; Gabor et al. 2011). At smaller masses, this model produces too vigorous early star formation in dwarfs, resulting in too-old stellar populations, too steep mass functions, and insufficient star formation today (a result also seen in many SAMs, e.g. Fontanot et al. 2009; Guo & White 2010). This may indicate that feedback in these dwarf systems evolves in some way not captured by this particular outflow prescription, or else that there is some additional physical process that is important. It is possible that the star formation law is different in smaller systems to make gas consumption less efficient (e.g. Robertson & Kravtsov 2008), or else that these simulations have too low a density threshold for star formation (owing to resolution limitations) such that they do not properly represent star formation in low surface brightness, gas-rich systems (e.g. Governato et al. 2010). More broadly, none of our simulations can simultaneously reproduce the shallow stellar mass function, archaeological downsizing, and star formation rate downsizing as observed; this remains a fundamental challenge for galaxy formation models. Even though the concordant mass range of the momentum-conserved wind model is fairly narrow, it is still a significant step forward as it provides physical insights into the processes that govern galaxy evolution at all masses, pinpointing both successes and failures. And it is worth recognizing that this particular dex in stellar mass happens to be where most of cosmic star formation occurs, so it is a critical mass range for understanding global stellar mass growth.

Overall, the general simulation-inspired framework for how inflows and outflows govern galaxy formation is compelling from both an observational and theoretical perspective, and is well-situated within the current hierarchical structure formation paradigm. This makes it an attractive scenario to pursue both analytically and numerically. In Paper II we will examine how this framework provides intuition about the gaseous and metal content of galaxies, thereby together covering the primary constituents that determine the observable multi-wavelength properties of galaxies at all cosmic epochs.

## ACKNOWLEDGEMENTS

The authors acknowledge A. Dekel, M. Fardal, M. Haas, N. Katz, D. Kereš, J. Kollmeier, C. Papovich, and D. Weinberg for helpful discussions, S. Weinmann for useful comments on an early draft, J. Schaye for helpful refereeing, and V. Springel for making GADGET-2 publicly available. RD thanks North West University in Mafikeng, South Africa and the University of Cape Town, South Africa for their hospitality during much of the writing of this paper. The simulations used here were run on University of Arizona's SGI cluster, ice. Support for this work was provided by NASA through grant number HST-AR-11751 from the Space Telescope Science Institute, which is operated by AURA, Inc.

under NASA contract NAS5-26555. This work was also supported by the National Science Foundation under grant numbers AST-0847667 and AST-0907998. Computing resources were obtained through grant number DMS-0619881 from the National Science Foundation.

## REFERENCES

- Agertz, O. et al. 2007, *MNRAS*, 380, 963
- Baldry, I. K., Glazebrook, K., Driver, S. P. 2008, *MNRAS*, 388, 945
- Baldwin, J. A., Phillips, M. M., Terlevich, R. 1981, *PASP*, 93, 5
- Balogh, M. L., Pearce, F. R., Bower, R. G., Kay, S. T. 2001, *MNRAS*, 326, 1228
- Bell, E. F., McIntosh, D. H., Katz, N., & Weinberg, M. D. 2003, *ApJS*, 149, 289
- Benson, A. J., Bower, R. G., Frenk, C. S., White, S. D. M. 2000, *MNRAS*, 314, 557
- Benson, A. J. 2010, *PhysRep*, in press, arXiv:1006.5394
- Berlind, A. et al. 2003, *ApJ*, 593, 1
- Bouche, N. et al. 2010, *ApJ*, 718, 1001
- Bouwens, R. J., Illingworth, G. D., Franx, M., Ford, H. 2007, *ApJ*, 670, 928
- Brinchmann, J., Charlot, S., White, S. D. M., Tremonti, C., Kauffmann, G., Heckman, T., Brinkmann, J. 2004, *MNRAS*, 351, 1151
- Chabrier G., 2003, *PASP*, 115, 763
- Chieffi, A. & Limongi, M. 2004, *ApJ*, 608, 405
- Conroy, C., Wechsler, R. H., Kravtsov, A. V. 2006, *ApJ*, 647, 201
- Crain, R.A., McCarthy, I.G., Schaye, J., Frenk, C.S., Theuns, T. 2010, *MNRAS*, submitted, arXiv:1011.1906
- Croton, D. J., et al. 2006, *MNRAS*, 365, 11
- Daddi, E. et al. 2007, *ApJ*, 670, 156
- Dai, X., Bregman, J. N., Kochanek, C. S., Rasia, E. 2010, *ApJ*, 719, 119
- Dalla Vecchia, C., Schaye, J. 2008, *MNRAS*, 387, 1431
- Davé, R., Gardner, J., Hernquist, L., Katz, N., Weinberg, D. 2000, in proc. “Clustering at High Redshift”, eds. A. Mazure, O. Le Fèvre, and V. Le Brun, *ASPC*, 200, p.173
- Davé, R. et al. 2001, *ApJ*, 552, 473
- Davé, R., Finlator, K., Oppenheimer, B. D. 2006, *MNRAS*, 370, 273
- Davé, R., Finlator, K., Hernquist, L., Katz, N., Kereš, D., Papovich, C., Weinberg, D. H. 2006, in “The Fabulous Destiny of Galaxies”, proc. Vth Marseilles Cosmology Conference, eds. V. Le Brun, A. Mazure, S. Arnouts and D. Burgarella, *Pars:Frontier Group*, p.219
- Davé, R., Oppenheimer, B. D. 2007, *MNRAS*, 374, 427
- Davé, R. 2008, *MNRAS*, 385, 147
- Davé, R., Oppenheimer, B. D., Sivanandam, S. 2008, *MNRAS*, 391, 110
- Davé, R., Oppenheimer, B. D., Katz, N., Kollmeier, J. A., Weinberg, D. H. 2010, *MNRAS*, in press, arXiv:1005.2421
- Davé, R. 2010, in proc. “UP2010: Have Observations Revealed a Variable Upper End of the Initial Mass Function?”, eds. M. Treyer, J.C. Lee, M.H. Seibert, T. Wyder, J. Neil, arXiv:1008.5283
- Davé, R., Finlator, K., Oppenheimer, B. D., Fardal, M., Katz, N., Kereš, D., Weinberg, D. H. 2010, *MNRAS*, 404, 1355
- Davé, R. 2009, in proc. “Galaxy Evolution: Emerging Insights and Future Challenges”, arXiv:0901.3149
- Dekel, A. & Silk, J. 1986, *ApJ*, 303, 39
- Dekel, A., Birnboim, Y. 2006, *MNRAS*, 368, 2
- Dekel, A. et al. 2009, *Nature*, 457, 451
- Di Matteo, T., Springel, V., Hernquist, L. 2005, *Nature*, 433, 604
- Dutton, A. A., van den Bosch, F. C., Dekel, A. 2010, *MNRAS*, 405, 1690
- Eggen, O. J., Lynden-Bell, D., Sandage, A. R. 1962, *ApJ*, 136, 748
- Elbaz, D. et al. 2007, *A&A*, 468, 33
- Finlator, K., Davé, R., Papovich, C., Hernquist, L. 2006, *Apj*, 639, 672
- Finlator, K. & Davé, R. 2008, *MNRAS*, 385, 2181
- Finlator, K., Oppenheimer, B. D., Davé, R. 2010, *MNRAS*, in press
- Firmani, C., Avila-Reese, V., Rodriguez-Puebla, A. 2010, *MNRAS*, in press
- Fontana, A. et al. 2006, *A&A*, 459, 745
- Fontanot, F., De Lucia, G., Monaco, P., Somerville, R. S., Santini, P. 2009, *MNRAS*, 397, 1776
- Förster Schreiber, N. M. et al. 2009, *ApJ*, 706, 1364
- Gabor, J. M., Davé, R., Finlator, K., Oppenheimer, B. D. 2010, *MNRAS*, 407, 749
- Gabor, J. M., Davé, R., Oppenheimer, B. D., Finlator, K. 2011, *MNRAS*, submitted, arXiv:1012.3166
- Geach, J. E., Smail, I., Best, P. N., Kurk, J., Casali, M., Ivison, R. J., Coppin, K. 2008, *MNRAS*, 388, 1473
- Genel, S., et al. 2011, *ApJL*, submitted
- González, V., Labbé, I., Bouwens, R. J., Illingworth, G., Franx, M., Kriek, M., Brammer, G. B. 2010, *ApJ*, 713, 115
- González, V., Labbé, I., Bouwens, R. J., Illingworth, G., Franx, M., Kriek, M., 2011, *ApJL*, submitted, arXiv:1008.3901
- Governato, F. et al. 2010, *Nature*, 463, 203
- Guo, Q. et al. 2010, *MNRAS*, accepted, arXiv:1006.0106
- Haas, M. 2010, Ph.D. Thesis
- Hayes, M., Schaerer, D., Östlin, G. 2010, *A&A*, 509, L5
- Hinshaw, G. et al. 2009, *ApJS*, 180, 225
- Hong, S., Katz, N., Davé, R., Fardal, M., Kereš, D., Oppenheimer, B. D. 2010, *MNRAS*, submitted, arXiv:1008.4242
- Hopkins, P. F., Quataert, E., Murray, N. 2011, *MNRAS*, submitted, arXiv:1101.4940
- Jogee, S. et al. 2009, *ApJ*, 697, 1971
- Kajisawa, M. et al. 2009, *ApJ*, 702, 1393
- Katz, N. & Gunn, J. E. 1991, *ApJ*, 377, 365
- Katz, N., Weinberg, D. H., Hernquist, L. 1996, *ApJS*, 105, 19
- Kauffmann, G., White, S. D. M., Heckman, T. M., Ménard, B., Brinchmann, J., Charlot, S., Tremonti, C., Brinkmann, J. 2004, *MNRAS*, 353, 713
- Kennicutt, R. C. 1998, *ApJ*, 498, 541
- Kennicutt, R. C. 1998, *ARA&A*, 36, 189
- Kereš, D., Katz, N., Weinberg, D. H., & Davé, R. 2005, *MNRAS*, 363, 2
- Kereš, D., Katz, N., Fardal, M., Davé, R., Weinberg, D. H. 2009, *MNRAS*, 395, 160
- Kereš, D., Katz, N., Davé, R., Fardal, M., Weinberg, D. H.

- 2009, MNRAS, 396, 2332
- Kimm, T. et al. 2009, MNRAS, 394, 1131
- Kitayama, T., Suto, Y. 1996, ApJ, 469, 480
- Kroupa, P. 2001, MNRAS, 322, 231
- Labbé, I. et al. 2010, ApJL, 716, L103
- Lee, J. C., Kennicutt, R. C., Funes, J. G., Sakai, S., Akiyama, S. 2009, ApJ, 691, 1305
- Leitner, S. N. & Kravtsov, A. V. 2010, ApJ, submitted, arXiv:1011.1252
- Li, I. H. et al. 2010, MNRAS, accepted, arXiv:1010.1447
- Ly, C., Lee, J. C., Dale, D. A., Momcheva, I., Salim, S., Staudaher, S., Moore, C. A., Finn, R. 2010, ApJ, submitted, arXiv:1011.2759
- Mac Low, M.-M., Ferrara, A. 1999, ApJ, 513, 142
- Maraston, C., Pforr, J., Renzini, A., Daddi, E., Dickinson, M., Cimatti, A., Tonini, C. 2010, MNRAS, 407, 830
- Marchesini, D., van Dokkum, P. G., Förster Schreiber, N. M., Franx, M., Labbé, I., Wuyts, S. 2009, ApJ, 701, 1765
- Martin, C. L. 2005, ApJ, 621, 227
- Martin, D. C. et al. 2005, ApJL, 619, L59
- McKee, C. F. & Ostriker, J. P. 1977, ApJ, 218, 148
- McGaugh, S. S., Schombert, J. M., de Blok, W. J. G., Zargursky, M. J. 2010, ApJL, 708, L14
- Mihos, J. C. & Hernquist, L. 1996, ApJ, 464, 641
- Mo, H. J., Mao, S., White, S. D. M. 1998, MNRAS, 295, 319
- Muñoz, J. A., Loeb, A. 2011, ApJ, submitted, arXiv:1010.2260
- Murali, C., Katz, N., Hernquist, L., Weinberg, D. H., Davé, R. 2002, ApJ, 571, 1
- Murray, N., Quatert, E., Thompson, T. A. 2005, ApJ, 618, 569
- Murray, N., Ménard, B., Thompson, T. A. 2010, ApJ, submitted, arXiv:1005.4419
- Nath, B. B. & Silk, J. 2009, MNRAS, 396, L90
- Neistein, E., van den Bosch, F. C., Dekel, A. 2006, MNRAS, 372, 993
- Noeske, K. G. et al. 2007, ApJL, 660, L43
- Nordon, R. et al. 2010, A&A, 518, L24
- Oppenheimer, B. D., Davé, R., Kereš, D., Katz, N., Kollmeier, J. A., Weinberg, D. H. 2010, MNRAS, 860, in press
- Oppenheimer, B. D. & Davé, R. 2006, MNRAS, 373, 1265
- Oppenheimer, B. D. & Davé, R. 2008, MNRAS, 387, 577
- Oppenheimer, B. D. & Davé, R. 2009, MNRAS, 395, 1875
- Oppenheimer, B. D., Davé, R., Finlator, K. 2009, MNRAS, 396, 729
- Papovich, C., Finkelstein, S. L., Ferguson, H. C., Lotz, J. M., Giavalisco, M. 2010 MNRAS, submitted, arXiv:1007.4554
- Pasquali, A., Gallazzi, A., Fontanot, F., van den Bosch, F. C., De Lucia, G., Mo, H. J., Yang, X. 2010, 407, 937
- Rasmussen, J., Sommer-Larsen, J., Pedersen, K., Toft, S., Benson, A., Bower, R. G., Grove, L. F. 2009, ApJ, 697, 79
- Rees, M. J., & Ostriker, J. P. 1977, MNRAS, 179, 541
- Robertson, B. E., Kravtsov, A. V. 2008, ApJ, 680, 1083
- Rupke, D. S., Veilleux, S., & Sanders, D. B. 2005, ApJS, 160, 115
- Salim, S. 2007, ApJS, 173, 267
- Scannapieco, E. & Bildsten, L. 2005 ApJ, 629, L85
- Schaye, J. et al. 2010, MNRAS, 402, 1536
- Schaerer, D., de Barros, S. 2010, A&A, 517, 73
- Schmidt, M. 1959, ApJ, 129, 243
- Simha, V., Weinberg, D. H., Davé, R., Gnedin, O. Y., Katz, N., Kereš, D. 2009, MNRAS, 299, 650
- Somerville, R. S., Hopkins, P. F., Cox, T. J., Robertson, B. E., Hernquist, L. 2008, MNRAS, 391, 481
- Springel, V. & Hernquist, L. 2003, MNRAS, 339, 289
- Springel, V. & Hernquist, L. 2003, MNRAS, 339, 312
- Springel, V. 2005, MNRAS, 364, 1105
- Stark, D., Ellis, R. S., Bunker, A., Bundy, K., Targett, T., Benson, A., & Lacy, M. 2009, ApJ, 697, 1493
- Steidel, C. C. et al. 2010, ApJ, 717, 298
- Tacconi, L. J. et al. 2010, Nature, 463, 781
- Thielemann, F.-K., Nomoto, K., & Yokoi, K. 1986, A&A, 158, 17
- van den Bosch, F. C. 2008, MNRAS, 387, 79
- van de Voort, F., Schaye, J., Booth, C. M., Haas, M. R., Dalla Vecchia, C. 2010, MNRAS, submitted, arXiv:1011.2491
- Weiner, B. J. et al. 2009, ApJ, 692, 187
- Weinmann, S. M., van den Bosch, F. C., Yang, X., Mo, H. J. 2006, MNRAS, 366, 2
- White, S. D. M., & Rees, M. J. 1978, MNRAS, 183, 341
- White, S. D. M. & Frenk, C. S. 1991, ApJ, 379, 52
- Yoshida, M., Kawabata, K. S., Ohya, Y. 2010, PASJ, submitted, arXiv:1012.1503
- Zhang, D. & Thompson, T. A. 2010, ApJ, submitted, arXiv:1005.4691